Wolin, Ryder, Leprince, Milke, Mowrer, Torero, Measurements of Smoke Characteristics in HVAC Ducts, Fire Technology 37(4), pp. 363-395, 2001

Measurements of Smoke Characteristics in HVAC Ducts

Steven D. Wolin, Noah L. Ryder, Frederic Leprince,
James A. Milke*, Frederick W. Mowrer and Jose L. Torero
Department of Fire Protection Engineering
University of Maryland
College Park, MD 20742-3031

* Corresponding Author: Address: 0151 Glenn Martin Hall, Department of Fire Protection Engineering, University of Maryland, College Park, MD20742-3031, USA. Telephone: 1-301-405-3995, FAX: 1-301-405-9383, e-mail: milke@eng.umd.edu

Wolin, Ryder, Leprince, Milke, Mowrer, Torero, Measurements of Smoke Characteristics in HVAC Ducts, Fire Technology 37(4), pp. 363-395, 2001

Abstract

The characteristics of smoke traveling in an HVAC duct have been observed along with the response of selected duct smoke detectors. The simulated HVAC system consists of a 9 m long duct, 0.45 m in diameter. An exhaust fan is placed at one end of the duct and is capable of inducing airflow rates that range from 0 to 1.5 m^3/s. The flow is controlled by means of a manual damper. On the upstream end of the duct there is a square exhaust hood approximately 2.2 m at the bottom and 0.3 m at the top. The bottom of the hood is approximately 2.5 m above the floor a shroud extends down to approximately 1.5 m above the floor. The test section, placed immediately downstream of the hood, is 3.5 m long duct with a square cross section of 0.4 m on a side. The instrumentation includes oxygen, carbon monoxide and carbon dioxide gas analyzers and a load cell to determine the energy release rate of the fires tested. The smoke within the duct is characterized by means of a laser light sheet and CCD camera, two white light source and photocell ensembles, a Pitot tube and an array of eight thermocouples placed on the vertical plane of symmetry. A smoke detector was placed at the downstream end of the test section. Two types of detectors were tested, ionization and photoelectric, with a single sampling probe geometry. The fires tested cover a wide range of fuels (propane, heptane, toluene, toluene/heptane mixture, shredded paper, polyurethane foam, wood cribs) with the peak energy release rates up to 800 kW. The smoke detector performance, temperature, flow field, smoke particle size and particle distributions are dependent on the fire characteristics and airflow through the duct. The different measurements could be scaled by means of the fire size and airflow rate but left a strong dependency on the fuel and burning characteristics (i.e. smoldering, flaming). The optical density and mass optical density are analyzed as metrics for characterizing smoke and smoke detector response. Detailed comparisons between the different metrics used are presented throughout this work. Clear evidence of stratification and aging of the smoke along the duct are also presented. The limitations of the present configuration and the need for a larger scale study are also discussed.

Wolin, Ryder, Leprince, Milke, Mowrer, Torero, Measurements of Smoke Characteristics in HVAC Ducts, Fire Technology 37(4), pp. 363-395, 2001

Introduction

The active spread of smoke by the heating, ventilation, and air-conditioning (HVAC) system in the event of a fire has been a concern for many years. The purpose of a duct smoke detector is to provide for shutdown of the HVAC system in the event of a fire to avoid actively re-circulating smoke through a building.

Extensive research has been conducted in the area of fire detection, with excellent general summaries provided by Grosshandler (1995, 1997), Mulholland (1995), Schifiliti (1995) and Milke (1999). Nevertheless, little work has been conducted into the effectiveness of duct smoke detectors. In light of the lack of research there has been only anecdotal evidence of their efficacy. The placement of duct smoke detectors has been based on rules, rather than analysis of performance. It has been suggested that the dilution of the smoke produced by a fire is so great that only fires that could be characterized as "major involvement," would trigger duct detector response. There has been little evidence to either support or refute the effectiveness of duct smoke detectors.

Currently, the Underwriters Laboratories (UL) listing process provides the principal test of the effectiveness of a duct smoke detector (1997, 1998). The test is not intended to evaluate the sensitivity of the detector response to different parameters related to the fire but to give an assessment of relative performance. For this purpose several common fire scenarios have been defined to test the detector performance as compared to that of a standard measuring ionization chamber. Tests are conducted for rigorously defined optical densities obtained with a white light source. The fire tests performed as part of the UL listing process for duct smoke detectors essentially consist of tests with two different fuel sources over a range of five air flow velocities. The fuels used are smoldering Ponderosa pine sticks and flaming n-heptane pool fires. The fire size is varied depending upon the flow rate of the test. Velocities range from 1.52 to 20.32 m/s in the duct section where the detector is mounted. The rate of buildup of smoke is required to stay within specified limits based upon optical density measurements made with a white light source and selenium barrier-layer type photocell and the output current of a measuring ionization chamber.

The relationship between the optical density measurements in the duct and the response of the duct smoke detector is not a direct one. The optical density is a constant

that is evaluated by measuring the decay in light intensity as a function of the path, representing a global measurement that incorporates complex effects such as forward scattering and absorption (van de Hulst (1981), Mulholland (1995) and Quintiere (1982)). Smoke detectors are traditionally of two types, ionization and photoelectric. Ionization detectors work on the principle of a current drop generated by the presence of smoke in an electrical field induced by a radioisotope and photoelectric by detecting light scattered by the smoke in a specific direction (Schifiliti (1995)). The optical density is not a direct measure of either mechanism of detection, resulting in great confusion when evaluating detector performance. This confusion has led to great controversy in the comparative assessment of the performance of different detectors (Meland and Lovnik (1991), Johnson and Brown (1986), Schifiliti (1995), Spearpoint and Smithies (1997)).

Significant work has been conducted to establish better metrics for detector performance. The optical density is not only difficult to correlate with the detector output but also depends on many variables intrinsic to the fire, such as fire size, fuel and ventilation. In an effort to eliminate the fire size and ventilation as variables, the optical density can be normalized leading to a constant that the fire community terms "mass optical density." The mass optical density has been found to be independent of fire size and ventilation conditions. Furthermore, it has been measured to be fairly constant for different fuels (Quintiere (1982), Seader and Einhorn (1977)).

The above approach has been questioned many times mainly due to inaccuracies generated by the way the measurements are conducted. Classical optical density measurements (UL (1997, 1998)) are done using a polychromatic light source. Analysis of the light obscuration measurement requires the use of Bouguer's law (Van de Hulst, 1981). Bouguer's law is strictly valid for light of a single wavelength greater than the size of the scattering particle. Therefore, precise measurements require the use of a monochromatic light source with a wavelength larger than the largest expected smoke particle size (Mulholland et. al. (2000) and Putorti, 1998). These studies have also shown that corrections for forward scattering of light are necessary and depend on the characteristics of the individual particles.

The integral nature of the measurement has also been a matter of concern. Mulholland (1995) points out that the mass optical density varies throughout the

trajectory of the smoke and shows that the specific extinction coefficient is a complex function of the smoke particle size distribution. The smoke size distribution evolves due to changes in the nature of the smoke, i.e. agglomeration and coagulation (aging of the smoke) (Mulholland, 1995) or simply due to uneven distribution of the smoke. The effect of aging of the smoke on the mass optical density can be significant and its evaluation by means of a polychromatic light source leads to significant error (Mulholland and Croarkin (2000)) but can be effectively quantified using a monochromatic light source (Clark (1985), Dobbins et. al. (1994)). Although aging is an issue of concern, for pool fires, it has been found that aging of smoke occurs very early and progresses little after the smoke leaves the fire (Levine, 1976). This supports the assumption that the mass optical density remains invariant once the smoke leaves the fire (Quintiere, 1982).

Several studies have been conducted to describe the characteristics of smoke particles. Mechanisms related to coagulation of smoke in fire plumes have been described by Baum and Mulholland (1979) and experimental studies have explored soot oxidation and agglomeration (Ezekoye and Zhang (1997), Hoffmann and Koopmann (1996), Hoffmann and Koopmann (1997)). Sophisticated techniques have been developed to characterize smoke and establish properties such as size distributions (Lee and Mulholland (1977), Mulholland and Ohlemiller (1982), Cashdollar et al. (1977)), scattering properties of smoke (Chung and Dunn-Rankin (1996)) or particle flow interactions (Gonzalez et al. (2000)). Alternative metrics from complex experimental arrangements have been proposed in the literature but they have not proven viable for practical applications.

Despite this wealth of information and the many problems associated with the current protocols, the optical density remains the norm when characterizing smoke detectors mainly due to the simplicity of its determination. The present study provides an in-depth evaluation of the current metrics for the application of HVAC smoke detectors. The use of the mass optical density as a proper criterion for assessment of detector performance is studied systematically by varying the three main variables affecting it: fuel, ventilation and fire size. Alternate metrics are used to identify possible limitations of this approach and to explain differences that can be attributed to phenomena such as flow stratification and aging.

Description of the Experimental Facility

A schematic diagram of the experimental facility is presented in Figure 1. This facility consists of a fully instrumented 3 m long duct (test section) connected on the upstream side to a square hood (approximately 2 m x 2 m) and on the downstream side to a 6 m duct leading to a fan that can provide a nominal range of airflow velocities of 0 to 10 m/s. A throttling device adjusts the airflow rate in the duct. Flanges provide a transition from the 0.45 m diameter round cross-section of the rest of the duct system to the 0.4 m square cross-section.

The test section has 3 sets of openings for optical access. At each location openings are made in all four sides of the duct. Each opening is 0.12 m in width and covers almost the entire 0.4 m of the test section. The openings can be covered by metal plates or by Pyrex windows depending on the measurement to be conducted. As shown in Figure 1, one set of openings is placed at each end of the test section and one in the middle. Windows are sealed to the duct using a high temperature RTV type sealant. One window of each set can be removed by pulling a cutting wire through the RTV sealant creating a gasket. The window is reattached using metal clips. This system allowed for the cleaning of all four of the viewing windows at that location with the removal of only one window. In order to reduce the reflection of light within the duct and allow for more precise optical measurements to be made, the inside of the duct is painted with high temperature matte black paint.

Eight type-K (24-gauge) thermocouples are mounted in the duct just downstream of the middle set of viewing windows (approximately 1.5 m from the upstream entrance to the test section). The thermocouples are mounted horizontally with the bead on the plane of symmetry with one end of the wires extending to either side of the duct. The wires penetrate small holes drilled in the side of the duct and are held in place using a strip of metallic tape. The beads form a vertical array, where each thermocouple is separated by 50 mm with bottom and top thermocouple 25 mm from the ceiling and floor of the test section. The purpose of the thermocouples is to provide a representative temperature distribution along the vertical plane of symmetry of the duct.

Commercially available duct smoke detectors are mounted to the duct at 2.30 m from the inlet flange along the length of the duct. Although a number of different

detectors are used, this paper only presents the results of one representative ionization detector and one light scattering photoelectric type detector to emphasize the objectives of this study. Each detector employs a sampling tube to direct air from the duct into a housing containing the detector. The discrete analog output from the sensors is stored on a computer providing a response curve from the detectors. The sampling tube is placed at the center point of the duct profile. The pressure difference between the inlet and outlet tubes on the duct detector housing is measured as a function of the flow rate in the duct prior to testing. The pressure difference is within the manufacturer's specifications for all flow rates used during testing.

The above measurements are complemented with oxygen consumption calorimetry, optical density measurements and two different types of video images of the light scattered by the smoke. The application of these techniques for this particular study required significant development, so detailed descriptions of the protocols and procedures follow.

Oxygen Consumption Calorimetry

Oxygen consumption calorimetry is applied within the present experimental configuration following the same methodology as that proposed by Huggett (1980), Parker (1984), Babrauskas (1984), Janssens (1991, 1995) and ASTM (1995(a)). The calibrated range of the system limits the maximum size of the fire for these experiments. Oxygen consumption calorimetry provides accurate results for an energy release rate up to approximately 350 kW. Nevertheless, a reduced number of tests are conducted with fires of an approximate size of 800kW. Details of the basic principles behind this approach are presented in the above references; therefore, this presentation is limited to describe the specific characteristics of the current experimental facility.

The energy release rate is the product of the mass of oxygen consumed during burning and 13.1 MJ/kg (of oxygen consumed) (Huggett (1980)). In order to calculate the oxygen consumption the mass flow rate of air taking part in the combustion process is determined. The mass flow rate of air taking part in the combustion process is determined indirectly by measuring the flow rate in the duct (Figure 1). A 0.34 m diameter orifice plate was installed in the duct system to determine the flow rate of

exhaust gases. Pressure taps are located before and after the orifice plate and are connected to the pressure transducer (Omega PX126 0 to 5 psi pressure transducer). This, along with the thermocouple installed within the duct near the orifice plate, allows the flow rate through the duct to be calculated.

To approximate the oxygen intake, the stoichiometry of the reaction is assumed. Stoichiometry of the process is incorporated by means of the expansion factor; a constant value of 1.105 is used for all fuels in this study (Janssens, 1995). The molecular weight of the exhaust gases is equated to the molecular weight of the air entrained into the fire.

Oxygen concentration measurements are performed using a Siemens Paramagnetic Oxymat 6 oxygen analyzer. Corrections due to incomplete combustion are incorporated by including in the calculations measurements of carbon monoxide and carbon dioxide obtained by means of a Siemens Ultramat 23 analyzer. Cooling of the hot exhaust gas in the sampling line and the sensitivity of paramagnetic oxygen analyzers to moisture require that the moisture in the sample gas be removed prior to analysis. Thus, gas concentration measurements are made on a dry basis, and a correction to all concentrations, due to the elimination of humidity, is incorporated in the calculations.

Preliminary experiments revealed a stratified flow within the duct upstream of the orifice plate. Because the inclusion of a mixing plate upstream of the orifice plate might have affected the flow measurement using the orifice plate and interfered with smoke measurements planned in the upstream portion of the duct, a mixing plate was not installed. Instead, two smaller holes were cut in the gas sampling tube to obtain samples across the duct cross-section and the sampling tube was moved downstream of the orifice plate. Experimental calibration of the calorimeter and comparison with data available in the literature (Tewarson, 1995) show this to be an acceptable sampling configuration, and therefore, errors due to stratification were assumed to be negligible.

The above measurements provide the time evolution of the oxygen consumed by the fire and thus of the energy release rate. Finally, the heat of combustion of the fuel can be determined by dividing the energy release rate by the mass loss rate. Placing the sample on a load cell (Automatic Timing and Controls load cell), mass loss rate and energy release rate can be measured simultaneously and the effective heat of combustion can be calculated as a function of time.

White Light Source Optical Density System

The system used to measure the optical density of the smoke in the duct consisted of a white light source and photocell mounted to the top and bottom of the duct. The system is similar to that used by UL for the measurement of optical density during the standard detector listing test (UL, 1997 and 1998). Thus, the optical density measurements made during these experiments are designed to be comparable, without correction, to those specified by UL. The quantitative results, however, cannot be compared directly because the size constraints and windows imposed by the test section result in differences. Nevertheless, the trends and conclusions presented throughout this work apply to the optical densities measured using the set-up proposed by UL.

The light source is a 6-volt rated (type 4515) automotive spotlight. The bulb was powered by a variable alternating current power supply run through a power conditioning circuit used to protect the bulb from overload. The power to the bulb was adjusted to 2.40 volts using a Fluke 75 Series II auto ranging multimeter. The photocell was a Weston model 594 photronic cell. The photocell is a selenium barrier-layer type with a 33 mm diameter active area. Output from the photocell was recorded using the same data acquisition system used for the calorimeter. The bulb and photocell were mounted to a single mounting bracket, which allowed for proper alignment of the two components and controlled adjustment of the bulb and the photocell relative to one another. The bracket could be moved to any of the three sets of windows along the length of the duct.

The light shone vertically through the duct to obtain an integral measurement of the obscuration. This measurement was intended to be a reference measurement to be compared with other parameters; therefore no horizontal measurements were made. While horizontal measurements at different heights could have been made, the Laser light sheet (described later), provides a more accurate representation of smoke stratification.

Smoke Characterization by Means of Light Scattering

Evaluation of light scattering by means of a CCD camera is used to establish a signature that is representative of the particle size and count. Light scatter is used because it provides a well-established correlation between the intensity of the scattered

light and particle size and density. Detailed description of the Mie theory for scattering can be found in the work of van de Hulst (1981) and will not be presented here.

Light scatter is a function of many variables; these include the view angle (θ) as measured from the direction of the light beam, the scattering cross section (C (cm^2)) and the ratio of the particle diameter to the wavelength ($\alpha = \pi D/\lambda$). Furthermore, the scattering cross section is strongly dependent on the geometry and composition of the particles. For proper interpretation of the signals collected, the intensity of the scattered light needs to be maximized. This makes the signal to noise ratio small and the results accurate. The constraints imposed by the duct and the strong concern for simplicity did not allow for an optimized signal to noise ratio. Nevertheless, the experimental set-up was designed to obtain the strongest signal within the bounds of the objectives of this study.

The intensity of the scattered light is proportional to the scattering cross-section (van de Hulst (1981)), which increases with the value of "α." Eckbreth (1988) shows the dependence of the cross section on "α" for carbonaceous particles. Particles from a wide range of fires have been shown to range between 0.05 μm and 5 μm (Lee and Mulholland, 1977) and their mean diameters between 0.4 μm and 3 μm (Mulholland, 1995), therefore, the light scattered from visible sources lead to values of "α" that range from approximately 0.2 to 25 for the entire range of particles, or 2 to 25 if the mean diameters are considered. Within this range the scattering cross section is large so the wavelength of the light source is of little relevance. Of more relevance is the maximum intensity produced by the light source.

Diode Lasers can be found in wavelengths that cover the entire visible spectrum, but the power to cost decreases with the wavelength. For this study a 500 mW SDL-7432-H1 diode Laser centered on 0.674 μm was used as the light source. This choice was made to maximize the power and to keep the light within the visible range. It is important to remain within the visible range so that a standard CCD camera can be used to record the light scattered by the particle.

The image acquisition process uses a monochrome COHU-4915 CCD video camera and zoom lens with a resolution of 752 pixels vertically and 480 pixels horizontally. The camera records the images in the RS-170/CCIR format. This

resolution provides a minimum pixel size of 10.02 μm vertically and 8.58 μm horizontally. A light filter centered at 0.678 μm and a bandwidth that ranges from 0.674 μm to 0.682 μm was used to minimize the contributions of ambient light.

Two cylindrical lenses produce a 10 mm wide light sheet that is approximately 1 mm in thickness across the view field of the camera. As shown in Figure 1, the light sheet is reflected on a 45^o mirror and directed from the bottom to the top of the duct. The light sheet is parallel to the side surfaces of the duct.

The image is captured at 90^o with the CCD camera (Figure 1) and the intensity recorded by each pixel represents a lumped estimation of the light scattered by the particles at a specific location. As mentioned before, the intensity of the scattered light depends on the view angle and is maximized for $\theta = 180^o$ (van de Hulst, 1981). Measurement of backward scattering is thus optimal for a point measurement. To obtain spatial distribution of the scattered light, and thus be able to define particle size and concentration, a compromise needs to be achieved between intensity and the deformation induced by the view angle. For this particular study the spatial resolution was prioritized, therefore, the view angle was set as perpendicular to the light sheet ($\theta = 90^o$).

Image processing of the recordings leads to a signature that is representative of size distribution and particle count. Since the particle images are not being captured directly this approach does not produce accurate measurements of quantity and size but, nevertheless, can provide a signature that can characterize the evolution of these variables with the different test parameters.

The computer used to capture the images and process them is a Pentium III 600 MHz machine equipped with an EPIX PIXCI imaging board that captures the images. The software used is XCAP image grabbing and treatment software.

Macroscopic Images

Images of the entire beam are obtained by means of the CCD camera and are used to determine the relative smoke density along a vertical line traversing the duct from top to bottom. If an invariant particle size distribution is assumed for the entire light sheet, then the light intensity recorded by the CCD camera can be directly related to the smoke particle quantity. The light intensity recorded by the camera can be interpreted as an indirect measurement of the particle concentration at each pixel. Assuming that the

particle size distribution remains invariant is reasonable since aging is expected to occur mostly in the stream-wise direction and not on the plane perpendicular to the flow. Wall effects as well as temperature variations across the cross-section of the duct might affect the particle size distribution, but are considered negligible. An accurate estimation of this error could be achieved by conducting local sampling of the smoke at different heights and establishing the particle size and density distributions. This calibration involves great experimental complexity (Mulholland, 1995); therefore, it was considered beyond the scope of this work. Nevertheless, while these measurements do not provide a quantitative estimate of the particle count, they do provide a relative evaluation of the particle concentration at each pixel location.

Smoke Signatures Obtained From a Magnified View of Light Scattering

A particle scatters light as it passes through the light sheet; the camera sees the scattered light. If the image captured by the camera is magnified sufficiently and the particle density is small, then the light scattered by a single particle can be recorded without overlaps with the light scatter by other particles. Under these conditions, analysis of the intensity recorded by each pixel can provide a signature of the number of particles within the field of view as well as the size of these particles.

The view from the camera, however, is not an actual measurement of the particle size but is a representative size. If the particle is much smaller than the pixel, then a single pixel is illuminated. As the particle increases in size, the intensity recorded by the pixel increases until the light scattered from the particle covers more than one pixel. In this case the pixels that neighbor the one containing the particle are also illuminated. Therefore intensity and the number of contiguous pixels illuminated provide an estimate of the particle size relative to the pixel size.

As noted previously, without magnification the dimensions of a pixel seen by the camera are approximately 10.02 μm vertically and 8.58 μm horizontally. Because the mean diameter of typical smoke ranges between 0.4 μm and 3 μm (Mulholland, 1995), magnification of at least 25 times is necessary to resolve the particles. The magnification required does not have to provide a resolution comparable to the particle size. The light intensity reaching a pixel is originated in a particle that is much smaller than what is

perceived by the camera (several diameters according to van de Hulst, 1981). Evaluation of the required magnification that provides pixel resolution for the projected size was performed under idealized conditions prior to the duct experiments showing that images recorded by the camera corresponded to 3-5 particle diameters.

To achieve this resolution a magnification system was developed. The magnification system consisted of two achromatic lenses in alignment. The magnification obtained is proportional to the ratio of the focal length of the second lens to the first. The characteristics of the camera and space constraints led to a maximum focal distance of 0.44 m. To obtain the required magnification, the lenses selected had an EFL = 50.29 mm and BFL = 60 mm for the first lens and an EFL = 394.33 mm and BFL = 400 mm for the second lense. The EFL is the focal distance measured from the surface of the lens and BFL is the focal length measured from the center of the lens. The magnification is given by the ratio of the EFL of the second to the first lens, which for this case results in a net magnification of 6.67. This combination of achromatic lenses and the cameras optical zoom provided a maximum pixel resolution of 1.29 μm horizontally and 1.50 μm vertically. This provides a pixel resolution on the same order as that of the image projected by the particles.

Extrapolation of the particle size can be done theoretically, but the precision of the results is questionable due to the uncertainty in the shape of the smoke particles. In contrast, direct comparison of the pixel illumination distribution with experimental data corresponding to well characterized fires could provide an adequate particle distribution. This calibration involves a complex arrangement (Mulholland, 1995) and therefore goes beyond the scope of the present work. In this study, the analysis will be done comparing the recorded images without defining the corresponding particle sizes.

Measurements of the representative particle sizes were made at the windows placed at the inlet and outlet of the duct (Figure 1).

Image Processing

The images obtained from the CCD camera through the image board provide an array of pixel intensities in the ASCII file format. The pixel intensity includes any background noise, which is present in the system due to dust, electronic interference, or

any other unknown source of noise. Averaging the measured intensities of 50 images captured under clean conditions (no smoke) and subtracting this mean noise from the measured intensities removes the background. Any pixel intensities with a negative value are considered as zero. Once the noise has been eliminated, two different treatments are performed to analyze the images obtained for these experiments.

For the macroscopic images the pixel values that will be presented correspond to an average of several images. A single image represents the instantaneous smoke distribution, therefore it might not be representative of the average conditions. It is therefore necessary to average a significant number of images that will lead to a proper representation of the average conditions. The number of images is limited by the evolution of the fire source, if the source evolves fast the number of images to be averaged has to be small, if the source has little or no evolution, the number of images can be increased significantly. Sources such as propane or heptane flames tend to attain steady conditions for time periods of the order of 30 to 60 seconds, allowing the use of a large number of images for the average. Others sources such as smoldering newspaper could never be considered steady-state in which case the number of images recorded and averaged had to be reduced.

Variations originating in passing smoke pockets are characterized by a high frequency, while changes in the fire source occur much slower so determination of the proper number of images to be averaged can be done from the observation of the time evolution of a single pixel. A smooth curve that follows the trend can be superimposed to the data and the number of points that has to be averaged to best reproduce the smooth curve can be determined. This can be validated as a function of time and for a number of different pixels. For the present study the number of images averaged to produce the quantitative data was always greater than 480 images (approximately 16 seconds of image recording).

Image processing was conducted on single images to determine the presence of a particle. The array of data corresponding to a single image show values ranging from 0 to 255, with 0 referring to black and 255 to white.

The particles are represented by pixels where the intensity is high due to the scattered light. But due to the angular dependency of the scattered light, the pixels on the

periphery will typically have a lower intensity than those in the "core" of the particle. This means that the particle must be represented as a square of pixels, which have the same approximate intensity. If the pixels do not have approximately the same intensity then it is most likely several particles and not just one.

In order to identify those combinations that truly are representative of a single particle two different methodologies are used. The first method chooses an arbitrary threshold to digitize an image. All intensity values above the threshold are identified as having a particle. Once the image is digitized, particles are counted using a Fortran subroutine developed specifically for this study. The subroutine counts the number of 1 by 1 pixel particles, 2 by 2 pixel particles, 3 by 3 pixel particles, and 4 by 4 pixel particles. The arbitrary threshold is increased and the process repeated until a significant change in particle counts is observed. Because all pixels within a particle have a similar intensity, once the change occurs the particle counts remain constant. The threshold at which the significant change occurs is taken as the threshold for the image. An average particle count is generated by averaging the individual counts of the same number of images used for the macroscopic view of the smoke.

A second methodology was used; this methodology relied on the same principles as the previous one but followed a different approach to identify the particles. An initial group of pixels (either 1 by 1, 2 by 2, 3 by 3 or 4 by 4 pixel squares) is identified. Within this group the pixel intensities are compared and if they match, within a specified percentage, the group is defined as an ensemble. The process starts with 4 by 4 boxes moving across the entire array a pixel at a time. Once the 4 by 4 ensembles have been identified, the unidentified areas are swiped by 3 by 3 ensembles, followed by 2 by 2 ensembles until the single pixels are identified. Once the ensembles are defined and average intensity is obtained for each ensemble, those ensembles with an average intensity above a specified threshold are counted as particles. The definition of the threshold is very clear because a broad gap is formed between those ensembles identified as particles and those identified as not being a particle. In contrast the percentage that defines an ensemble is difficult to establish. It was found that percentage differences between 10% and 15% provided the most consistent results. As for the other technique, a

particle count was generated for each image and then averaged over the same number of images used for the macroscopic view of the smoke.

The two techniques provided consistent results and were both applied to all experiments, but the second method was generally used to report the results. The second technique provides a better estimate of error since varying the percentage difference that defines the ensemble can serve as a sensitivity analysis. This was done to show that best results can be obtain if the error is defined between 10% and 15%.

Experimental Results

The objective of this study is to characterize the different variables that have a significant effect on the performance of a duct smoke detector. The variables chosen for the present experiments are the fuel, fire size and volumetric exhaust flow rate.

All of the different measurements described in the previous section were conducted simultaneously. The optical density system was placed at the opposite end of the duct from the Laser system. That is, for tests where the Laser system was positioned at the set of viewing windows at 30 cm, the optical density system was mounted at 300 cm. The commercial duct smoke detector was positioned with the sampling tube at 230 cm from the inlet for each test. A test was conduced for each fuel using a photoelectric and an ionization type duct smoke detector at each of four exhaust flow rates.

A total of 98 tests were conducted. Table 1 provides the conditions examined in each test series. A test series generally consists of tests over the range of airflow rates. The size of the fire (energy release rate) was varied from a few kW to approximately 800 kW. The volumetric flow rates examined were nominally 1.42, 1.07, 0.71, and 0.36 m^3/s. The highest flow rate is the maximum flow of the exhaust fan. The other three volumetric flow rates correspond to three-quarters, one-half, and one-quarter of the full volumetric flow rate. The fire sizes were chosen in order to allow tests to be conducted at each of the four flow rates without overflowing the hood and to allow for the full range of detector output to be examined. For the largest fire sizes tests could only be performed at the highest flow rate.

Fuel sources for the experiments were chosen to provide a wide range of smoke characteristics and allow for comparison to the UL listing criteria (1998). As an example, Figure 2 shows, two extreme cases. Figure 2(a) corresponds to a 45 cm diameter n-heptane fire, a flaming fire with a low soot yield, and Figure 2(b) shows a shredded newspaper smoldering fire representing the other extreme of the fires examined. The smoke from the shredded newspaper fire is predominately a liquid aerosol and the energy release rate is very low. Other test fuels were chosen for different reasons; toluene was chosen for its high soot yield and the relatively large smoke particle sizes. The mixture of toluene and n-heptane (25 % toluene / 75 % n-heptane) was also tested. This mixture is used in the UL room fire test of smoke detectors (UL, 1997). Flexible polyurethane

foam blocks and wood cribs (Douglas-Fir) were tested due to their common applications. Polyurethane foam is mainly used as furniture padding and is characterized by very fast flame spread rates. The wood cribs are the same as those specified as "Class A" (57 by 305 by 305 mm) and "Class B" (57 by 152 by 152 mm) cribs in the ASTM E108 test of roof coverings (ASTM, 1995(b)). Due to their slow spread rate the wood cribs were ignited using 300 mL and 100 mL respectively of methanol placed in a 150 mm diameter pan, 60 mm below the suspended crib.

The shredded newspaper test provides both a period of smoldering combustion, during which thick white smoke is produced, and a period of flaming combustion, during which almost no visible smoke is produced. The smoldering period is illustrated in Figure 2(b). A hollow steel cylinder 0.1 m in diameter and 0.3 m long is filled with 42 g of shredded newspaper. The shredded newspaper is packed into the bottom 200 mm of the cylinder and the cylinder is placed on a ring stand with a piece of wire mesh holding the contents of the cylinder in place. The newspaper is ignited touching the bottom center of the cylinder with a small flame. The ignition source is removed as soon as the production of smoke is observed, following the protocol used in UL 217 (UL, 1997).

A propane fire was run each day for the purpose of calibrating the calorimeter. Propane was run from a tank through a flow meter and then into a 60 cm diameter round burner filled with gravel. Test data was collected for all of the instruments during the propane calibrations.

Smoke Detector Response

The signal from two smoke detectors (one photoelectric type detector and one ionization type) was used to describe the effect that the three different variables have on the signal obtained from the detector. The signal was gathered directly from the detector and plotted as a function of time. Figures 3 and 4 show the detector response as a function of time and compared to the rate of energy released by the fire. Figure 3 corresponds to the output of a photoelectric detector to a flaming polyurethane foam fire and Figure 4 to an ionization detector exposed to the smoke of a fire generated by a mixture of 25% toluene and 75% n-heptane placed in a 0.15 m pan. As seen in both figures, the detector response closely follows the energy release rate. In the case of the

toluene/n-heptane mixture both curves follow almost identical trends and cover the same time span. Figure 3 shows that for the case of polyurethane foam, the detector continues to register a significant signal, even after the fire is extinguished. This is due to the smoking residue left after the flame ceases to exist. For a given fuel, the detector signal is proportional to the energy release rate and, thus to the size of the fire.

The effect of the airflow velocity through the duct on the detector output is shown in Figure 5. The response of an ionization detector is presented in Figure 5(a) and that of a photoelectric detector in Figure 5(b). As indicated in both figures, as the air velocity increases, the signal from the detector decreases due to dilution of the smoke. The relative signal from the ionization detector is generally larger than that obtained from the photoelectric one. The results presented correspond to several different tests; therefore, the time shift does not correspond to a delayed response from the photoelectric detector but to the time taken to start the experiment.

The final parameter to be studied is the fuel type. average detector responses for the different fuels used at a fixed optical density of 0.1 m^{-1} are presented in Figure 6. The detector response depends significantly on the fuel and the combustion mode. The extreme scenario of smoldering newspaper shows a strong response of the photoelectric detector compared to a very weak response of the ionization type detector. In contrast, the other extreme condition, flaming n-heptane shows the opposite trend. If toluene (high soot yield fuel) is present, both detectors will respond in a similar manner.

The above paragraphs showed that the fire size (Figures 3 and 4), dilution (Figure 5) and fuel type (Figure 6) affect the response of both photoelectric and ionization smoke detectors. In a later section, the effect of these same parameters on smoke characteristics is presented to assess the impact of fire size, dilution and fuel type on detector performance.

Mass Optical Density

Light obscuration was measured across the duct using a white light source following the recommendations given by UL (1997 and 1998). The measurements presented in this section were made at 3 m from the smoke intake (Figure 1). Measurements were also conducted at the inlet but followed the same trends. Further

discussion of the differences between the two locations will be presented in following sections.

An extinction coefficient or optical density is extracted from the attenuation of light by means of Bouguer's law.

$$\ln\left(\frac{I_{\lambda,L}}{I_{\lambda,0}}\right) = -\int_0^L K_\lambda dL \quad \text{or} \quad \log\left(\frac{I_{\lambda,L}}{I_{\lambda,0}}\right) = -\int_0^L D_\lambda dL \tag{1}$$

Where $I_{\lambda,L}$ is the attenuated intensity of radiation (W/m^2), $I_{\lambda,0}$ the source intensity of radiation (W/m^2), L the path length (m), D_λ the monochromatic optical density (m^{-1}) and K_λ the monochromatic extinction coefficient (m^{-1}). Both expressions are equivalent and can be integrated under the assumption that the optical density remains constant over the path length, L. Furthermore, for a white light source that consists of multiple wavelengths, the integration of equation (1) leads to an average optical density (D) or extinction coefficient (K)

$$\frac{I_{\lambda,L}}{I_{\lambda,0}} = e^{-KL} \quad \text{or} \quad \frac{I_{\lambda,L}}{I_{\lambda,0}} = 10^{-DL} \tag{2}$$

The optical density is therefore linked to the extinction coefficient by a factor of 2.303 where K/D=2.303. It is more common for fire related studies to use the optical density (D), therefore this parameter will be used for the analysis of the data.

It is important to state that the assumptions of a constant optical density through the path length and that an average optical density can be obtained from integration of equation (1) are difficult to support. The smoke density, and therefore the optical density, varies along the cross section of the duct. Horizontal measurements of the optical density at different heights along the duct conducted throughout this study showed that the variation of the optical density throughout the duct could be very significant and is intimately related to other variables of the problem such as the flow velocity and the fire size. Furthermore, Bouguer's law is strictly valid for light of a single wavelength (Van de Hulst, 1981). Many studies have shown that a monochromatic light with a wavelength larger than the largest expected particle size is necessary for precise measurements (Mulholland et. al. (2000) and Putorti, 1998). These studies have also shown that corrections for forward scattering of light are necessary and depend on the characteristics of the individual particles.

Despite these problems, an average optical density has been the norm when characterizing smoke detectors, mainly due to the simplicity of its determination. In the present study, this parameter is used as a benchmark, but the results are compared with more precise measurements. As detailed in the description of the experimental facility, the current optical measurements, other than the optical density, conform to the requirements defined by Mulholland et al. (2000) and Putorti (1998).

As an example, the evolution of the optical density (D) with the energy release rate for a 0.15 m Toluene fire is presented in Figure 7. A single fire is used to describe the different observations but the trends are similar for all experimental conditions. As the fire grows in size, the energy release rate and optical density grow in an analogous manner. A direct dependency of the optical density on the energy release rate can be extracted from Figure 7.

The fluctuations of the flame that can barely be observed from the energy release rates are very clear from the optical density measurements. Although there is a significant difference in the magnitude of the response of the different measurements to the fluctuations there is coincidence on the timing and frequency. The large size of smoke particles preclude them from following turbulent fluctuations, therefore, the diffusivity of these particles is less affected by turbulence, resulting in a particle distribution that is less homogeneous than the oxygen concentration used to obtain the energy release rate measurements. The smoke particles are more likely to follow the flame fluctuations and consequently the flame pulsating frequency will clearly show on the time evolution of the optical density.

A comparison of the energy release rate obtained from oxygen measurements with that obtained from the recorded mass loss is presented in Figure 8. At the location of the measurement, oxygen can be assumed to be well mixed therefore the fluctuations are attenuated. In contrast, mass loss follows the fluctuations of the flame. The optical density traces (Figure 7) thus resemble more those of the energy release rate obtained through an average heat of combustion (Tewarson (1995) (Figure 8). In contrast, Figure 7 shows that the timing of optical measurements conducted at 3 m from the inlet tends to correspond with the energy release rate calculated from oxygen consumption measurements. Figure 8 shows a time delay between the energy release rate obtained

from the fuel mass loss and that calculated from oxygen consumption measurements. Therefore, the mass loss measurements are used to isolate the effect of fire size from the optical density, but all times are adjusted using a time delay equivalent to the delay between the two measurements of the energy release rate.

Figure 9 shows the dependence of the optical density on the flow velocity. An increase of the airflow through the duct will result in dilution of the smoke and a decrease in the average optical density. If the fire is too large, the dependence of the optical density on the airflow changes because the extraction system cannot take in all of the air entrained by the fire. Because fires that significantly overwhelm the flow within the duct provides results that depend on the characteristics of the particular set-up, these results cannot be generalized to other scenarios and thus set the limits for the fire size.

Based on the information extracted from Figures 7 and 9, the optical density, D [1/m], can be assumed to be proportional to the mass of smoke moving through the control volume ($\dot{m}_f$ [g/s]) and inversely proportional to the airflow rate ($\dot{V}$ [m^3/s]). The constant of proportionality is generally termed the mass optical density (D_m [m^2/g]). The above statements can be expressed mathematically in the following form:

$$D = D_m \frac{\dot{m}_f}{\dot{V}} \tag{3}$$

Quintiere (1982) and Seader and Einhorn (1977) present an analytical justification to equation (3). The analysis presented by Quintiere (1982) and Seader and Einhord (1977) shows that the mass optical density can be expressed by

$$D_m = \frac{\sigma_S y_S}{2.303} \tag{4}$$

Where σ_s (m^2/g) is the specific extinction coefficient and y_S is the soot yield. The constant of 2.303 comes from the conversion from extinction coefficient to optical density. The specific extinction coefficient is a function of the structure of the soot particles and can be considered dependent only on the fuel. Similarly, the soot yield can be considered a function only of the burning fuel. In summary, the mass optical density can be deemed a function only of the fuel.

Based on the above arguments, equation (3) can be used to calculate the mass optical density from the measurements presented in Figures 7 and 9. Mulholland (1995)

proposes that the mass optical density will vary throughout the trajectory of the smoke. Mulholland (1995) shows that the specific extinction coefficient is a complex function of the smoke size distribution, which evolves due to agglomeration and coagulation (Mulholland, 1995). This process is termed aging of the smoke. For pool fires, aging of the smoke has been found to occur very early and progress little after the smoke leaves the fire (Levine, 1976), which supports the assumption that the mass optical density remains invariant once the smoke leaves the fire (Quintiere, 1982). Nevertheless, collection of smoke into a duct precludes dilution and enhances turbulence, thereby promoting aging. Thus, the observations by Mulholland (1995) regarding the effect of aging on the mass optical density need to be considered with great attention in this study. Indeed, throughout the present experiments, it was found that under identical experimental conditions the optical density measured at the inlet of the duct differed from measurements conducted 3 m downstream.

In this section only data obtained 3 m downstream is presented. No attempt is made to define the effect of aging on mass optical density since Mulholland and Croarkin (2000) have shown that polychromatic light results in significant discrepancies in the evaluation of the specific extinction coefficient. In contrast, Mulholland and Croarkin (2000) and Dobbins et. al. (1994) showed very consistent results when a monochromatic light source was used. Therefore, the monochromatic light source (i.e. Laser) is used to study the evolution of the smoke along the duct.

The mass optical density measured 3 m downstream of the duct for a 0.15 m toluene fire is presented in Figure 10 for the four airflows studied. The mass optical density tends to increase slightly over the course of the experiments, reaching approximately 0.1 m^2/g after approximately 150 seconds. This delay corresponds well with the establishment of a quasi-steady flow within the duct. Towards the end of the fire the mass loss tends to zero resulting in artificial fluctuations of the mass optical density.

An average mass optical density was calculated for different fuels, different fire sizes and different flows. The mass optical densities obtained for all conditions for each fuel were averaged and the averages are presented in Figure 11. Figure 11 shows that the mass optical density for Toluene is significantly larger than values obtained for other fuels, with polyurethane foam having the lowest value. Smoldering newspaper

measurements have a large uncertainty since the combustion reaction transitioned cyclically between smoldering and flaming.

Except for toluene, all other average mass optical densities can be found within the error bars. The large accumulation of soot that occurred on the duct windows for the tests conducted with toluene can explain this difference. Throughout an experiment the duct windows accumulated soot increasing the light obscuration. For most experiments this increase can be compensated by assuming that the enhanced obscuration has a linear dependency with time. The data can thus be corrected by obtaining a reference optical density measurement at the beginning and at the end of the test. This correction was effective for most of the cases studied, leading to an almost constant mass optical density towards the end of the test (Figure 10). For toluene fires greater than 0.15 m in diameter, even with the correction the mass optical density continued to increase due to a significant accumulation of soot on the windows. The same observation also was made for the largest n-heptane fire (0.6 m). Because this drift was much more significant with toluene than with n-heptane at comparable energy release rates, indicates that the drift was related to the characteristics of the smoke and not to the effect of the fire on the flow within the duct.

The average values presented in Figure 11 are based on all of the mass optical density measurements obtained for energy release rates above 5 kW. Criteria for data rejection would have been arbitrary and therefore post processing of the data was not performed. The large values of the mass optical density for toluene can be attributed to the drift problem.

Particle Counts

This section presents pixel counts for different experimental conditions to further address the effects of fire size, dilution and fuel type on the characteristics of the smoke within the duct. These measurements can be expected to provide a more accurate description of the smoke, since the experimental methodology is free of many of the approximations implied in the optical density measurements stipulated by UL (1997 and 1998). All the data presented in this section corresponds to a single location in the duct (3 m from the inlet and 0.1 m from the top of the duct).

The evolution of the pixel counts as a function of time is presented in Figure 12. The 1 x 1 pixel counts are presented in Figure 12(a) and 2 x 2 pixel counts in Figure 12(b). Larger pixel counts were obtained and showed similar trends. Trends become more difficult to identify as the number of counts decreases, therefore larger pixel counts are not presented here. The experimental data corresponds to a 0.15 m n-heptane fire. Figures 12(a) and 12 (b) show that the number of pixel counts increases with the energy release rate. Fluctuations in the energy release rate are followed by similar changes in the number of pixel counts, but with a slight time delay. When normalizing the pixel data all times were adjusted using a time delay equivalent to the delay between the two measurements of the energy release rate.

The evolution of the 1 x 1 pixel counts for different airflow rates for a 0.15 m 25% Toluene/75% n-Heptane fire is presented in Figure 13. Each data point presented corresponds to 30 image count averages. Data was taken for approximately 60 seconds at a period where the energy release rate was almost steady. As shown for the detectors (Figure 5) and for the optical density (Figure 9), an increase in the flow rate results in a decrease in the number of pixel counts as well as a decrease in the optical density and detector response.

Figures 12 and 13 show that the normalization that leads to the mass optical density (equation (3)) is also appropriate for the pixel counts. Because the light source is monochromatic (0.674 μm), errors associated with the effect of wavelength on light attenuation and incorporated in the integration of equation (1) are minimized. Furthermore, the scattered light is measured at 90^{o} by the CCD camera to enable forward scattering to be neglected.

The pixel counts obtained for different tests were, normalized by the fuel mass loss rate and the airflow velocity per equation (3). As an example, data obtained for the five n-heptane fires ranging from 50 kW to 200 kW is presented in Figure 14. With the exception of the earlier and later stages of the test where the energy release rate tends towards zero, the normalized pixel counts are consistently at approximately 0.8×10^{5} $[m^3/g]$. The average values for all seven fuels are presented in Figure 15.

Because average pixel counts can be obtained for periods as short as a few seconds, data could be gathered for conditions where mass optical density showed

dramatic error bars (i.e. wood cribs, flaming newsprint). Furthermore, extremely sooty flames such as toluene could be addressed by short measurements conducted at different stages of the fire where the windows would be cleaned and measurements obtained immediately after.

In Figure 15, the normalized pixel counts and the mass optical density follow the same trends for all fuels studied. Single pixel counts (1 x 1) and four pixel counts (2 x 2) follow almost identical trends. The large discrepancy in the mass optical density between toluene and other fuels is not present in the normalized pixel counts. Toluene thus appears to produce very similar smoke to the mixture of 25% toluene/75% n-heptane, verifying the hypothesis that this discrepancy is introduced by the accumulation of soot on the duct windows.

Comparison of figures 6 and 15 show that the correlation between the performance of photoelectric detectors and pixel counts is very good. This is expected since the principle by which photoelectric detectors operate is very similar to the present measurements. In contrast, the present measurements do not correlate as well with the output of ionization detectors.

Spatial Evolution of the Smoke

The previous section described measurements conducted at a specific location within the duct. These measurements helped to identify the effects of dilution, fire size and fuel. Altering the location of the measurement resulted in a significant variation in the results providing evidence of changes in the nature of the smoke as it progressed through the duct (aging) and an unequal distribution of the smoke across the cross section of the duct (stratification). The size constraints of the present facility do not allow for a systematic study of these parameters, but this section will attempt to qualitatively illustrate their importance.

Stratification

Three different measurements were made to study flow stratification within the duct, velocity measurements, temperature measurements and 90^{o} scattered

monochromatic light recorded by a CCD camera. The geometric constraints of the facility precluded making all three measurements at the same location, therefore velocities and temperatures where obtained 1.5 m downstream of the inlet and scattering measurements where obtained at the inlet and at 3 m downstream.

All three measurements resulted in consistent information. Nevertheless, it was clear that many variables affected the structure of the flow within the duct and the effects of fire size, fuel and airflow could not be completely isolated. The scattering measurements showed a significant evolution of the particle distribution between the inlet and 3 m downstream. Because measurements could not be made further along the duct of the current experimental facility, the possibility of the observed stratification being an inlet effect could not be confirmed or refuted. Because the inlet was open to the fire, the nature of the burning fuel had a significant effect on the initial condition and thus on the evolution of the flow along the duct. As an example, the data from a 0.15 m n-heptane fire is used in this paper to illustrate the correlation between the different measurements. Details of these measurements can be found in Ryder (2000) and Wolin (2000).

Figure 16 shows the velocity distribution along the vertical center-plane of the duct. The data is presented normalized, the vertical distance from the flow, y, is normalized by the height of the duct, H, and the velocity by the nominal velocity (i.e. flow rate divided by the duct area). Data is presented for the maximum and minimum flow rates and for both, a 35 kW fire and the cold flow. In the absence of a fire the air flows parallel to the longitudinal axis of the duct. The velocity distribution shows a slight increase at the top of the duct that is due mostly to the inlet condition. Nevertheless, the divergence from the mean is less than 5%, which is within experimental error for the nature of the Pitot tube used for these experiments. No measurements could be made close to the wall due to the intrusiveness of the probe.

In the presence of a fire, the flow accelerates at the top of the duct. The velocity overshoot is more significant for the low flow velocity case (~40%) decreasing as the velocity reaches its maximum value (~20%). Stratification occurs when buoyancy dominates over the flow inertia, therefore the effects of buoyancy (stratification) are reduced as the airflow velocity increases.

Further evidence of stratification can be obtained from the temperature measurements (Figure 17). The temperatures are scaled by means of a characteristic temperature:

$$\theta = \frac{T - T_\infty}{\Delta T_C} \tag{5}$$

Where T_∞ is the ambient temperature and the characteristic temperature is obtained by delivering the entire energy release rate ($\dot{Q}$) into the mass flow of air ($\dot{m}_a = \rho_\infty \dot{V}$) and calculating the temperature rise that will be generated ($\Delta T_C = \dot{Q} / \dot{m}_a c_{P\infty}$). The specific heat is that of air at ambient temperature ($c_{P\infty}$).

Figure 17 shows that for low airflows (0.36 m^3/s) the energy of the fire is concentrated in the top part of the duct. As the flow increases the energy is better distributed along the duct. For comparison, the averaged CCD recordings of the scattered light are also shown in Figure 17. The intensity recorded by each pixel in a vertical line that goes from top to bottom is recorded and normalized by the saturation value (255). The normalized intensity values obtained for several images are then averaged. The averaged intensity distributions across the duct for 0.36 m^3/s and 1.42 m^3/s, presented in Figure 17, show an accumulation of smoke particles at the top of the duct. The particles seem to be more concentrated towards the top than energy and mass. This could be attributed to the low diffusivity of the particles, in contrast with a higher diffusivity for the gases and energy. Earlier results related to the energy release rate have provided evidence of reduced mixing of smoke as opposed to oxygen, therefore a similar interpretation could be used to explain the differences between scattered light and temperature and velocity measurements. In addition, further experimental evidence is necessary where all of the measurements are collected at the same location. However, the differences could also be attributed to the evolution of the smoke along the duct.

The effects described above do not disappear as the fire decreases in size. Very small fires still show a variation of the temperature, velocity and smoke particle density across the duct, but the trends are far from clear. In contrast, as the fire size increases the flow begins to deform showing two velocity peaks, one close to the bottom of the duct and a second one at the top. Smoke and temperature measurements seem to follow the

same trends. Eventually, when the fire saturates the flow and smoke starts accumulating in the hood, the importance of the two peaks decreases and all indicators show a well mixed flow within the duct.

Aging

All of the different measurements pointed to an evolution of the smoke along the duct. This evolution can be divided into two different aspects, the evolution of the flow and the evolution of the smoke particles. The previous section showed that the flow mixes as it progresses through the duct and evidence of this evolution could be obtained from the temperature, velocity and smoke particle density. As the flow mixes the nature of the smoke particle changes; and this can be seen in the evolution of the particle counts. Figures 18 and 19 show normalized measurements of particle counts for 1 x 1 and 2 x 2 pixel counts respectively for different n-heptane fires. Only data corresponding to n-heptane will be presented as an example, with similar trends observed for all fuels studied. These measurements were taken at the same height from the base of the duct and in a region where the average intensity of the scattered light was similar. Again, direct comparison of these results is difficult since particle size and distribution affect the total scattered light and in these measurements both variables are being modified simultaneously. Independent of this reservation, the trends can be used to qualitatively assess the evolution of the smoke particles along the duct.

Comparison of the 1 x 1 particle counts (Figure 18) shows that the normalized particle counts are consistent for different fire sizes and flow velocities independent of the location within the duct. Nevertheless, the total counts decrease by almost an order of magnitude in 3 m. Furthermore, the artificial increase of the normalized particle counts as the energy release rate decreases is much less significant at the inlet than 3 m downstream. This is justifiable since time lags are more difficult to estimate as the distance between the fire and the measurement location increases. Particles remain within the duct increasing the number of counts towards the end of the test. Figure 19 shows an opposite trend for the larger counts. This trend is similar for all larger counts so only 2 x 2 pixel counts are used to describe this process. The normalized pixel counts increase by approximately 100 % in the 3 m distance between measurements. A simple

arithmetic analysis that considers that the mass and density of soot remain constant shows if 8 cubes of 1 pixel in side are attached together, a single cube of 2 pixels in side will result. This observation is consistent with the data presented in Figures 18 and 19 and leads to the interpretation that the changes in pixel count can be attributed to agglomeration of the soot particles along the duct.

Conclusions

An experimental study has been conducted to assess the variables that could affect detector performance in HVAC ducts. It has been shown that:

- For a specific fuel, the response of sample photoelectric and ionization detectors is directly related to the smoke concentration within the duct therefore can be considered proportional to the energy release rate (i.e. fuel mass burning rate) and inversely proportional to the airflow rate.
- There is a strong relationship between fuel and detector response. Furthermore, for the same fuel, smoldering combustion significantly increases the response of a photoelectric detector and has the opposite effect on an ionization detector.
- The present study only used sample detectors therefore the above conclusions cannot be generalized to all detectors and should be used only as reference measurements to establish the context for this work. The current paper is part of a larger study that addresses the variability of these conclusions as a function of the specific characteristics of the detector.
- The use of optical density following the methodology established by UL (1997,1998) has been evaluated for an HVAC duct. When the optical density is normalized leading to a mass optical density, photoelectric detector response and mass optical density correlate well for flaming fires despite the limitations of the UL technique. Careful analysis of optical density measurements is necessary to prevent misleading results. For the present experiments, fuels with high soot yield such as toluene yield an overestimation of the mass optical density.
- For a specific fuel, the optical density is proportional to an ionization detector response. The mass optical density and ionization detector response do not correlate well when comparing different fuels.
- For smoldering newsprint the mass optical density is very similar to that of other flaming fuels, nevertheless the response of photoelectric detectors is much higher and that of ionization detectors is much lower.
- Monochromatic light scattered at 90^{o} and recorded by a CCD camera was used as a parallel metric to determine the effect of fuel, fire size and dilution on the characteristics of the smoke within an HVAC duct. For a specific fuel, the light

scattered at 90^o is also directly related to the smoke concentration within the duct and therefore can be considered proportional to the energy release rate (i.e. fuel mass burning rate) and inversely proportional to the airflow rate. Consequently, the data could be scaled in the same manner as the mass optical density.

- Monochromatic light scattered at 90^o correlates very well with photoelectric detector response, even for smoldering newsprint.
- For the particular ionization detectors studied, mass optical density and monochromatic light scattered at 90^o did not show a good correlation with detector response.
- Transition between smoldering and flaming fires lead to high uncertainty in the results. Similarly, highly evolving fires such as wood cribs resulted in large error bars.
- Within the constraints of the present experimental facility, velocity and temperature measurements showed important stratification of the flow. Monochromatic light scattered at 90^o also showed stratification, but the results cannot be directly compared because data could not be gathered at the same location within the duct.
- Within the constraints of the present experimental study, monochromatic light scattered at 90^o showed significant evolution of the smoke particles (aging) with the distance from the fire source.
- For the present study, aging and stratification are intimately related to the experimental facility; therefore these results require validation in a larger scale facility where the evolution of the flow can be tracked through a distance larger than 3 m.

Acknowledgements

This work was funded by the Fire Detection Institute. The suggestions and comments of John Cholin are greatly appreciated. The authors would like to

acknowledge the support to the experimental work of James Greene III, Shamim Rashid, Matthew Hulcher and a number of undergraduate students.

References

ASTM, "Standard Test Method for Heat and Visible Smoke Release Rates for Materials and Products Using an Oxygen Consumption Calorimeter," *1995 Annual Book of ASTM Standards*, Vol. 04.07, American Society for Testing and Materials, Philadelphia, PA, pp. 1114-1130, 1995(a).

ASTM, "Standard Test Methods for Fire Tests of Roof Coverings," 1995 Annual Book of ASTM Standards, Vol. 04.07, American Society for Testing and Materials, Philadelphia, PA, pp. 429-430, 1995(b).

Babrauskas, V., "Development of the Cone Calorimeter – A Bench-Scale Heat Release Rate Apparatus Based on Oxygen Consumption," *Fire and Materials*, Vol. 8, pp. 81-95, 1984.

Cashdollar, K.L., Lee, C.K. and Singer, J.M., "Smoke Particle Size and Concentration Measurements by a Three Wave Length Light Transmission Technique," The Eastern State section Meeting of the Combustion Institute, November 10-11, 1977.

Chung, I.-P. and Dunn-Rankin, D. "In Situ Light Scattering Measurements of Mainstream and Sidestream Cigarette Smoke," *Aerosol Science and Technology*, 24:85-101, 1996.

Clark, F.R.S., "Assessment of Smoke Density with a helium-Neon Laser," *Fire and Materials*, Vol. 9, No. 1, 1985.

Dobbins, R.A., Mulholland, G.W., and Bryner, N.P., "Comparison of a Fractal Smoke Optics Model with Light Extinction Measurements," *Atmospheric Environment*, Vol. 28, No. 5, pp. 889-897, 1994.

Eckbreth, A.C., "Laser Diagnostics for Combustion Temperature and Species," Abacus Press, A.K. Gupta and D.G. Lilley Editors, 1988.

Ezekoye, O. A. and Zhang, Z., "Soot Oxidation and Agglomeration Modeling in a Micro-gravity Diffusion Flame," *Combustion and Flame*, 100:127-139, 1997.

Gonzalez, I., Hoffmann, T.L. and Gallego, J.A., "Precise Measurements of Particle Entrainment in a Standing Wave Acoustic Field Between 20 and 3500 Hz," Journal of Aerosol Science, Vol. 31, 12, 1461-1468, 2000.

Grosshandler, W.L. "Proceedings of the 1995 Workshop on Fire Detector Research," NISTIR-5700, Gaithersburg, Maryland, 1995.

Grosshandler, W.L., "Progress Report on Fire Detection Research in the United States," U.S./Japan Government Cooperative Program on Natural Resources (UJNR), 13th Joint Panel Meeting, March 13 – 20, 1996, Gaithersburg, Maryland, Vol. 2, Beall, K.A., Ed., pp. 363-369, 1997.

Huggett, C., "Estimation of the Rate of Heat Release by Means of Oxygen Consumption," *Journal of Fire and Flammability*, Vol. 4, No. 2, pp. 61-65, 1980.

Hoffman, T.L. and Koopmann, G.H. "Visualization of Acoustic Particle Interaction and Agglomeration: Theory Evaluation," Journal of the Acoustic Society of America, 101, 6, 3421-3429, 1997.

Hoffman, T.L. and Koopmann, G.H. "Visualization of Acoustic Particle Interaction and Agglomeration: Theory and Experiments," Journal of the Acoustic Society of America, 99, 4, 2130-2141, 1996.

Janssens, M.L., "Measuring Rate of Heat Release by Oxygen Consumption," *Fire Technology*, Vol. 27, No. 3, pp. 234-249, 1991.

Janssens, M.L., "Calorimetry," *SFPE Handbook of Fire Protection Engineering*, 2nd ed., DiNenno, P.J., Ed., National Fire Protection Association, Quincy, MA, pp. 3-16-3-36, 1995.

Johnson, P.F. and Brown, S.K., "Smoke Detection of Smoldering Fires in a Typical Melbourne Dwelling," *Fire Technology*, vol. 22, 4, 1986.

Lee, T.G.K. and Mulholland, G. W., "Physical Properties of Smoke Pertinent to Smoke Detectors," NBSIR 77-1312, U.S. Department of Commerce, 1977.

Meland, O. and Lonvik, L.E., "Detection of Smoke: Full Scale Tests with Flaming and Smouldering Fires," Fire Safety Science-Proceedings of the Third International Symposium, 975-984, 1991.

Milke, J.A., "Monitoring Multiple Aspects of Fire Signatures for Discriminating Fire Detection," *Fire Technology*, Vol. 35, No. 3, 1999.

Mulholland, G. and Ohlemiller, T.J. "Aerosol Characterization of a Smoldering Source," *Aerosol Science and Technology*, 1:59-71, 1982.

Mulholland, G.W., "Smoke Production and Properties," SFPE Handbook of Fire Protection Engineering, 2nd ed., DiNenno, P.J., Ed., National Fire Protection Association, Quincy, MA, pp. 2-217-2-227, 1995.

Mulholland, G.W., Johnsson, E.L., Fernandez, M.G., and Shear, D.A., "Design and Testing of a New Smoke Concentration Meter," *Fire and Materials*, Vol. 24, pp. 231-243, 2000.

Mulholland, G.W., and Croarkin, C., "Specific Extinction Coefficient of Flame Generated Smoke," *Fire and Materials*, Vol. 24, pp. 227-230, 2000.

Parker, W., "Calculations of the Heat Release Rate by Oxygen Consumption for Various Applications," NBSIR 81-2427, National Bureau of Standards, Gaithersburg, MD, 1982.

Putorti, A.D., "Design Parameters for Stack-Mounted Light Extinction Measurement Devices," NISTIR 6215, National Institute of Standards and Technology, Gaithersburg, MD, July 1998.

Quintiere, J.G., "Smoke Measurements: An Assessment of Correlations between Laboratory and Full-scale Experiments," *Fire and Materials*, Vol. 6, Nos. 3 and 4, pp. 145-148, 1982.

Ryder, N. L. "Stratification and Aging Effects on Duct Smoke Detectors in HVAC Systems," Master of Science Thesis, University of Maryland, College Park, Maryland, 2000.

Schifiliti, R.P. Meacham, B.J., and Custer, R.L.P., "Design of Detection Systems," SFPE Handbook of Fire Protection Engineering, 2nd ed., DiNenno, P.J., Ed., National Fire Protection Association, Quincy, MA, p. 4-16 , 1995.

Seader, J.D., and Einhorn, I.N., "Some Physical, Chemical, Toxicological, and Physiological Aspects of Fire Smokes," 16th Symposium (International) on Combustion, Proceedings, The Combustion Institute, pp. 1423 – 1445, 1977.

Spearpoint M J and Smithies J N. "Practical comparison of domestic smoke alarm sensitivity standards." FRDG Publication Number 4/97, Home Office Fire Research and Development Group, 1997.

Tewarson, A., "Generation of Heat and Chemical Compounds in Fires," SFPE Handbook of Fire Protection Engineering, 2nd ed., DiNenno, P.J., Ed., National Fire Protection Association, Quincy, MA, pp. 3-71-3-79, 1995.

UL, "Standard for Safety for Single and Multiple Station Smoke Alarms, UL 217," 5th Ed., Underwriters Laboratories Inc., Northbrook, IL, 1997.

UL, "Standard for Safety 268A: Smoke Detectors for Duct Application," 3rd Ed., Underwriters Laboratories Inc., Northbrook, IL, 1998.

Van de Hulst, H.C., "Light Scattering by Small Particles," Dover Publications Inc., New York, 1981.

Wolin, S. D. "An Investigation of Optical Density, Oxygen Consumption Calorimetry and Duct Smoke Detection," Master of Science Thesis, University of Maryland, College Park, Maryland, 2000.

Table 1. List of Experiments

	Fuel	Comments	Detector	Laser Position
1	Propane	60 cm diameter burner	None	30 cm
2	Toluene	212 g in 15 cm pan - 1 test at full flow	None	30 cm
3	Propane	60 cm diameter burner	Photoelectric 1	30 cm
4	Heptane	150 g in 15 cm pan	Photoelectric 1	30 cm
5	Polyurethane Foam	18.5x29x15 cm block	Photoelectric 1	30 cm
6	Propane	60 cm diameter burner	Photoelectric 2	30 cm
7	Polyurethane Foam	26x16x16 cm block	Photoelectric 2	30 cm
8	Propane	60 cm diameter burner	Photoelectric 2	30 cm
9	25% Toluene 75% Heptane	150 g in 15 cm pan	Photoelectric 2	30 cm
10	Heptane	150 g in 15 cm pan	Photoelectric 2	30 cm
11	Propane	60 cm diameter burner	Photoelectric 2	30 cm
12	Propane	60 cm diameter burner	Photoelectric 3	30 cm
13	Propane	60 cm diameter burner	Photoelectric 3	30 cm
14	Small Wood Crib	152x152x57 mm Douglas Fir crib (ignition unsatisfactory)	Photoelectric 3	30 cm
15	Small Wood Crib	152x152x57 mm Douglas Fir ignited w/ 100 mL Methanol	Photoelectric 3	30 cm
16	Propane	60 cm diameter burner	Photoelectric 3	30 cm
17	Large Wood Crib	305x305x57 mm Douglas Fir ignited w/ 300 mL Methanol	Photoelectric 3	30 cm
18	Propane	60 cm diameter burner	Photoelectric 3	30 cm
19	Newspaper	42.6 g in 102 mm diameter by 305 mm long column	Photoelectric 3	30 cm
20	Propane	60 cm diameter burner	Photoelectric 4	30 cm
21	Heptane	150 g in 15 cm pan	Photoelectric 4	30 cm
22	Large Wood Crib	305x305x57 mm Douglas Fir ignited w/ 300 mL Methanol	Photoelectric 4	30 cm
23	Heptane	60 cm diameter pan	Photoelectric 4	30 cm
24	Propane	60 cm diameter burner	Photoelectric 4	30 cm
25	Toluene	150 g in 15 cm pan	Photoelectric 4	30 cm
26	Propane	60 cm diameter burner	Ionization 1	300 cm
27	Heptane	150 g in 15 cm pan	Ionization 1	300 cm
28	Heptane	45 cm pan - 1 test - full flow - no load cell	Ionization 1	300 cm
29	Propane	60 cm diameter burner	Ionization 1	300 cm
30	Propane	60 cm diameter burner	Ionization 1	300 cm
31	Small Wood Crib	152x152x57 mm Douglas Fir ignited w/ 100 mL Methanol	Ionization 1	300 cm
32	25% Toluene 75% Heptane	150 g in 15 cm pan	Ionization 1	300 cm
33	Propane	60 cm diameter burner	Ionization 2	300 cm

34	Polyurethane Foam	26x16x16 cm block	Ionization 2	300 cm
35	Propane	60 cm diameter burner	Ionization 2	300 cm
36	Newspaper	42.6 g in 102 mm diameter by 305 mm long column	Ionization 2	300 cm
37	Toluene	150 g in 15 cm pan	Ionization 2	300 cm
38	Toluene	800 g in 30 cm pan	Ionization 2	300 cm
39	Propane	60 cm diameter burner	Photoelectric 4	30 cm
40	Newspaper	42.6 g in 102 mm diameter by 305 mm long column - full flow	Photoelectric 4	30 cm
41	Heptane	45 cm pan on load cell - 1 test at full flow	Photoelectric 4	30 cm
42	Heptane	60 cm pan on load cell - 2 tests at full flow - spillover from hood	Photoelectric 4	30 cm

List of Figures

Figure 15 Average pixel counts normalized by the fuel mass burning rate [g/s] and the airflow velocity [m^3/s]. The data presented was obtained for different fuels and fires ranging from 50 kW to 200 kW. For comparison the mass optical density [m^2/g] is also presented. The pixel count data corresponds to measurements made at 3 m from the duct inlet.

Figure 16 Normalized velocity distribution along the plane of symmetry of the duct. Measurements were made at 1.5 m from the inlet and are normalized by the nominal flow rate.

Figure 17 Normalized intensity and temperatures along the plane of symmetry of the duct. A characteristic temperature calculated from the energy release rate was used to normalize the temperatures and the saturation value for a pixel (256) to normalize the intensity.

Figure 18 Pixel counts normalized by the fuel mass burning rate [g/s] and the airflow velocity [m^3/s]. The data corresponds to n-heptane fires ranging from 50 kW to 200 kW. The pixel count data corresponds 1 x 1 pixel counts and measurements made at the inlet and at 3 m downstream.

Figure 19 Pixel counts normalized by the fuel mass burning rate [g/s] and the airflow velocity [m^3/s]. The data corresponds to n-heptane fires ranging from 50 kW to 200 kW. The pixel count data corresponds 2 x 2 pixel counts and measurements made at the inlet and at 3 m downstream.

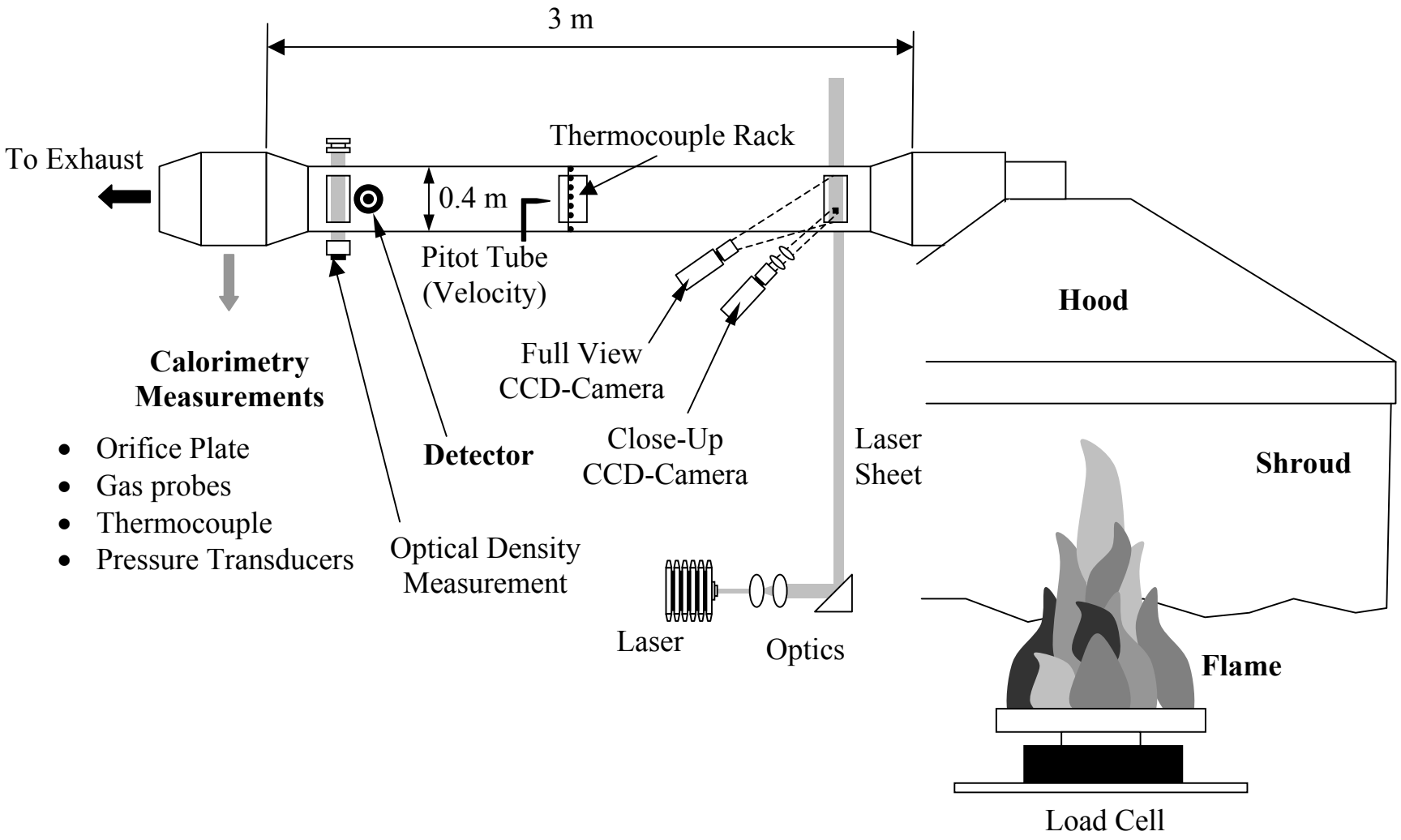

Wolin et al.
Figure 1

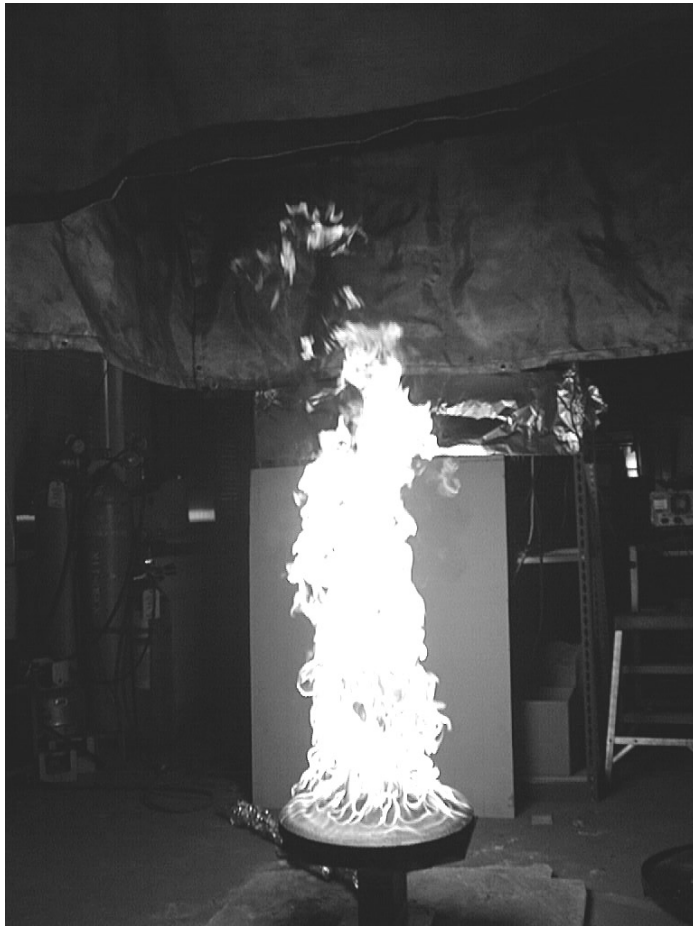

(a)

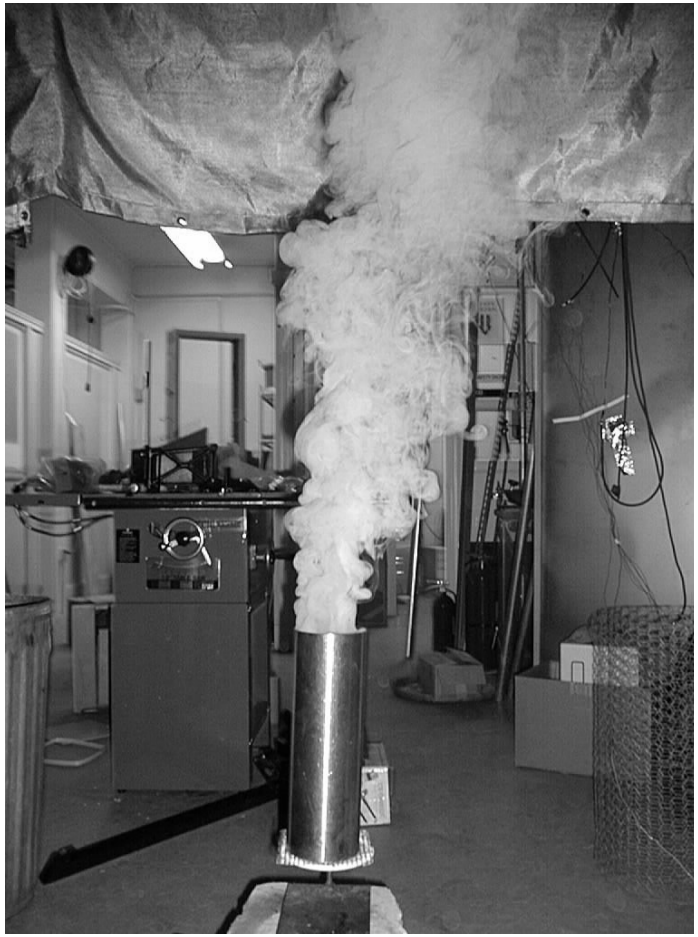

(b)

Wolin et al.
Figure 2

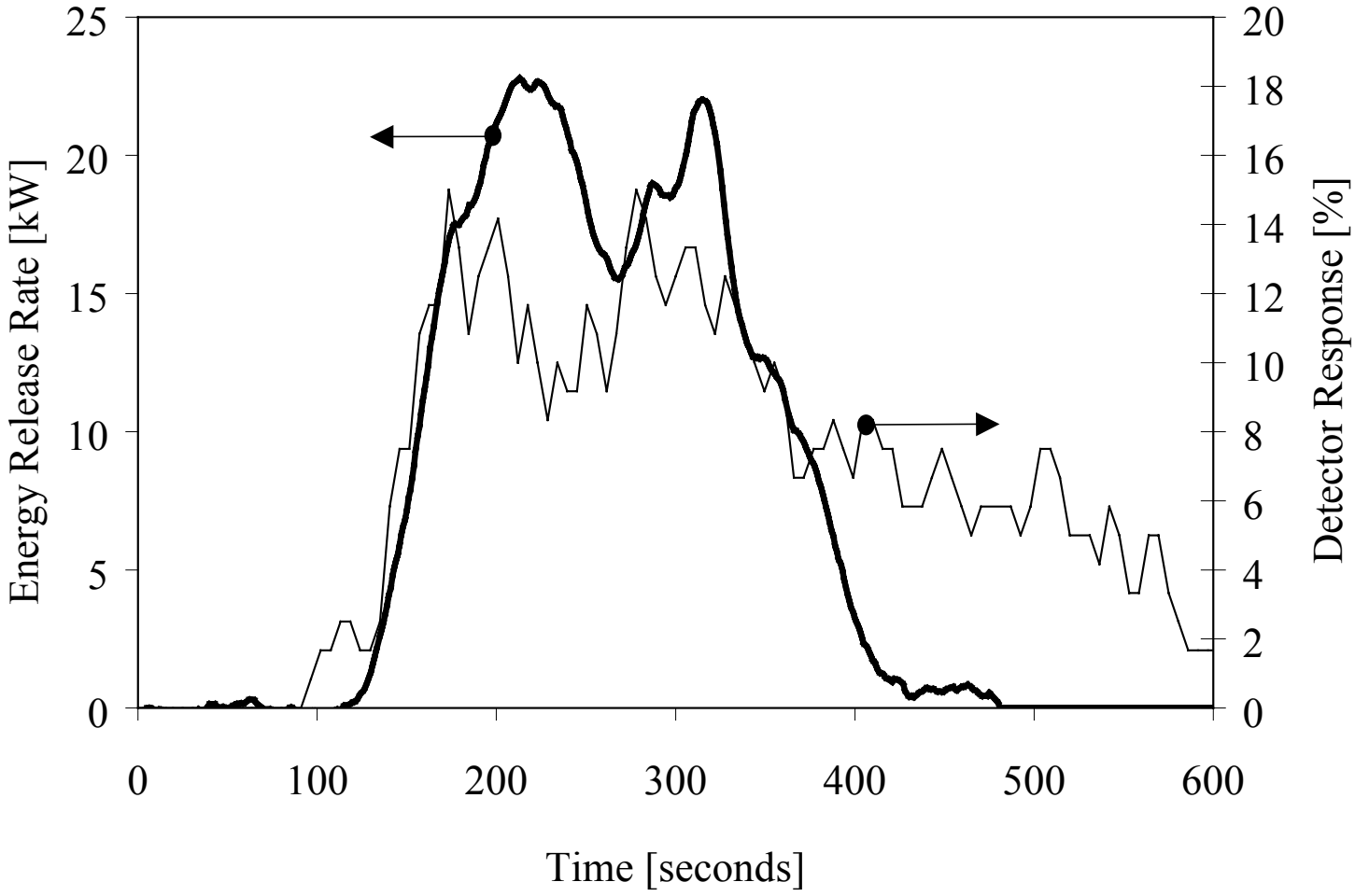

Wolin et al.
Figure 3

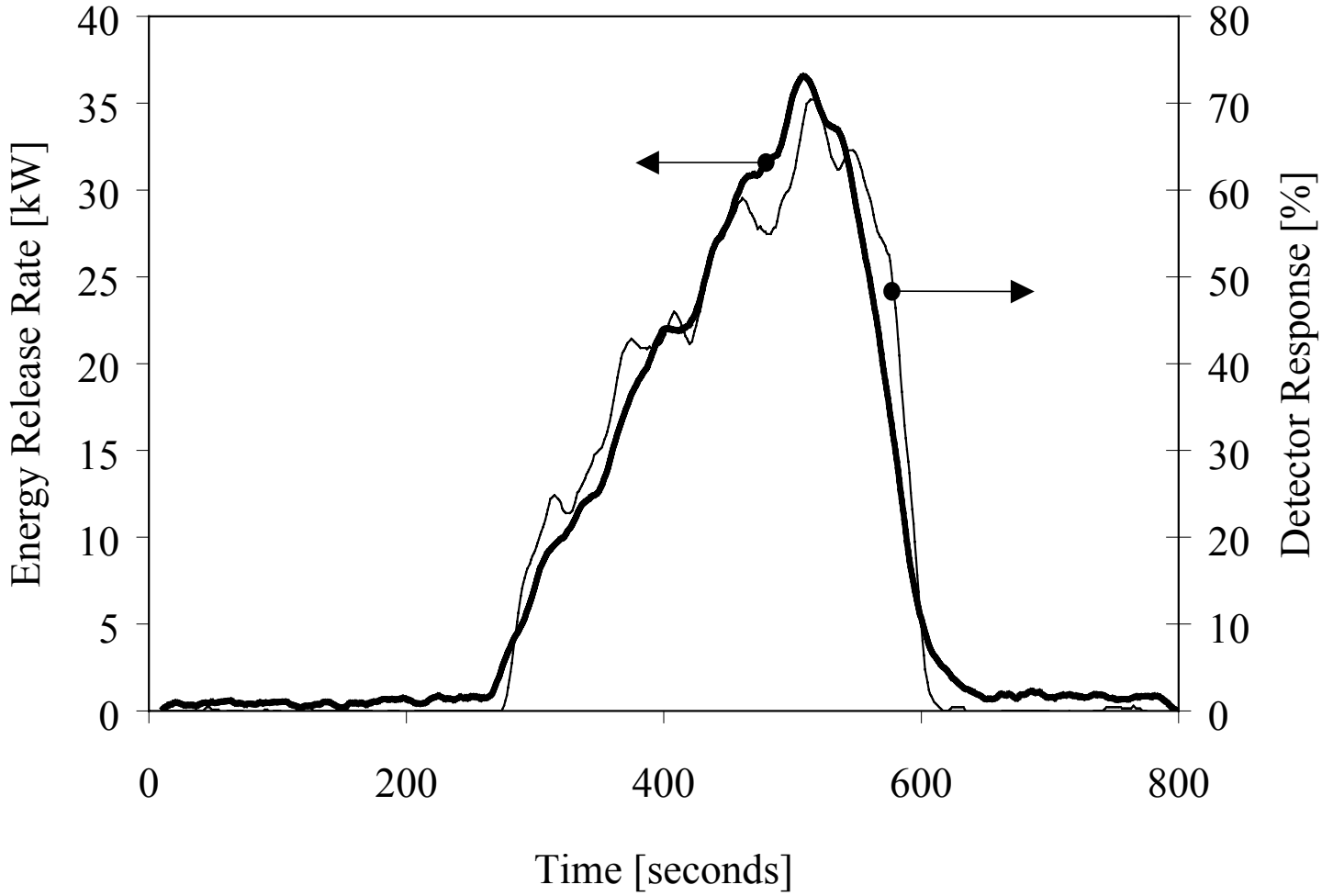

Wolin et al.
Figure 4

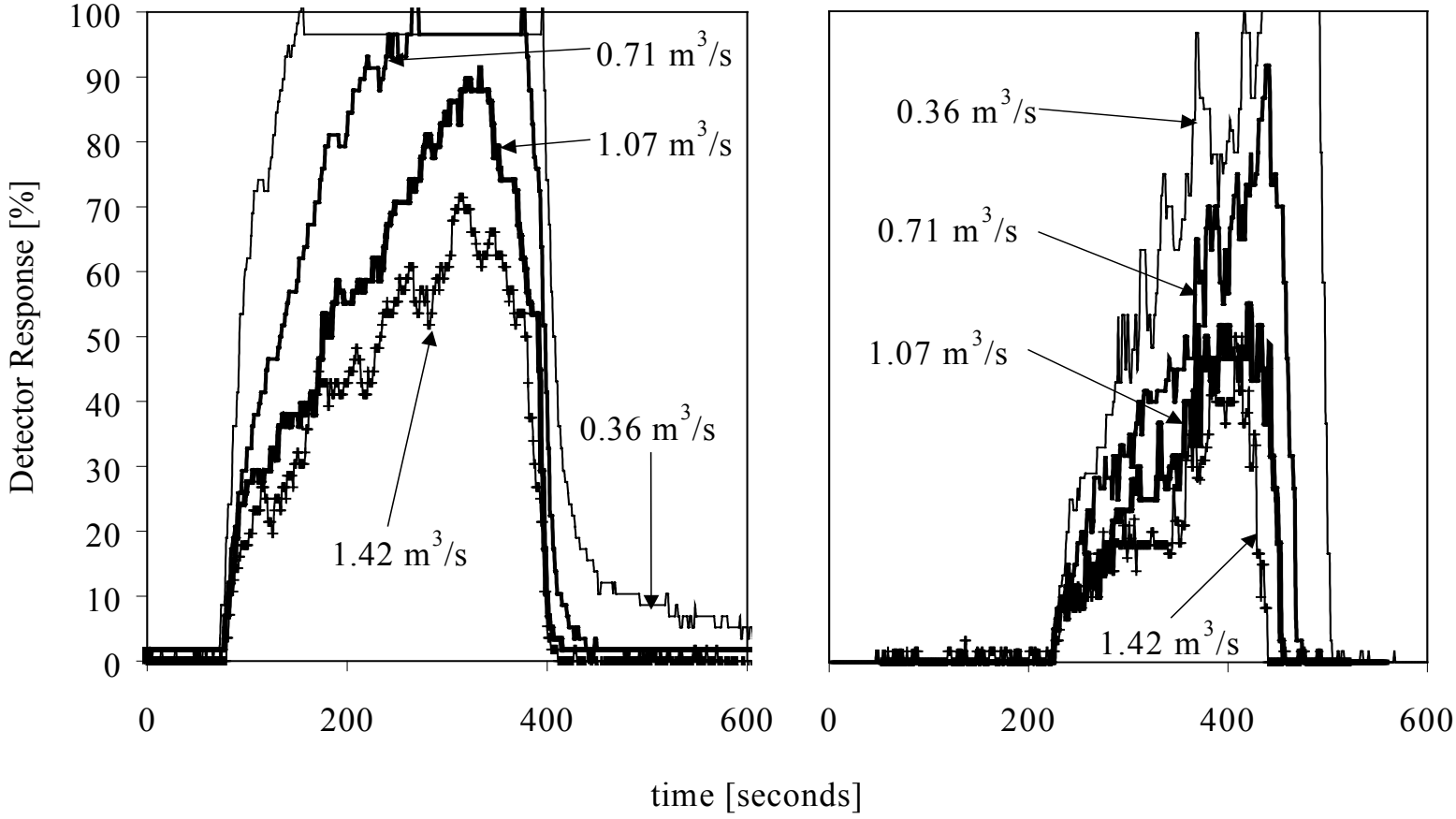

Wolin et al.
Figure 5

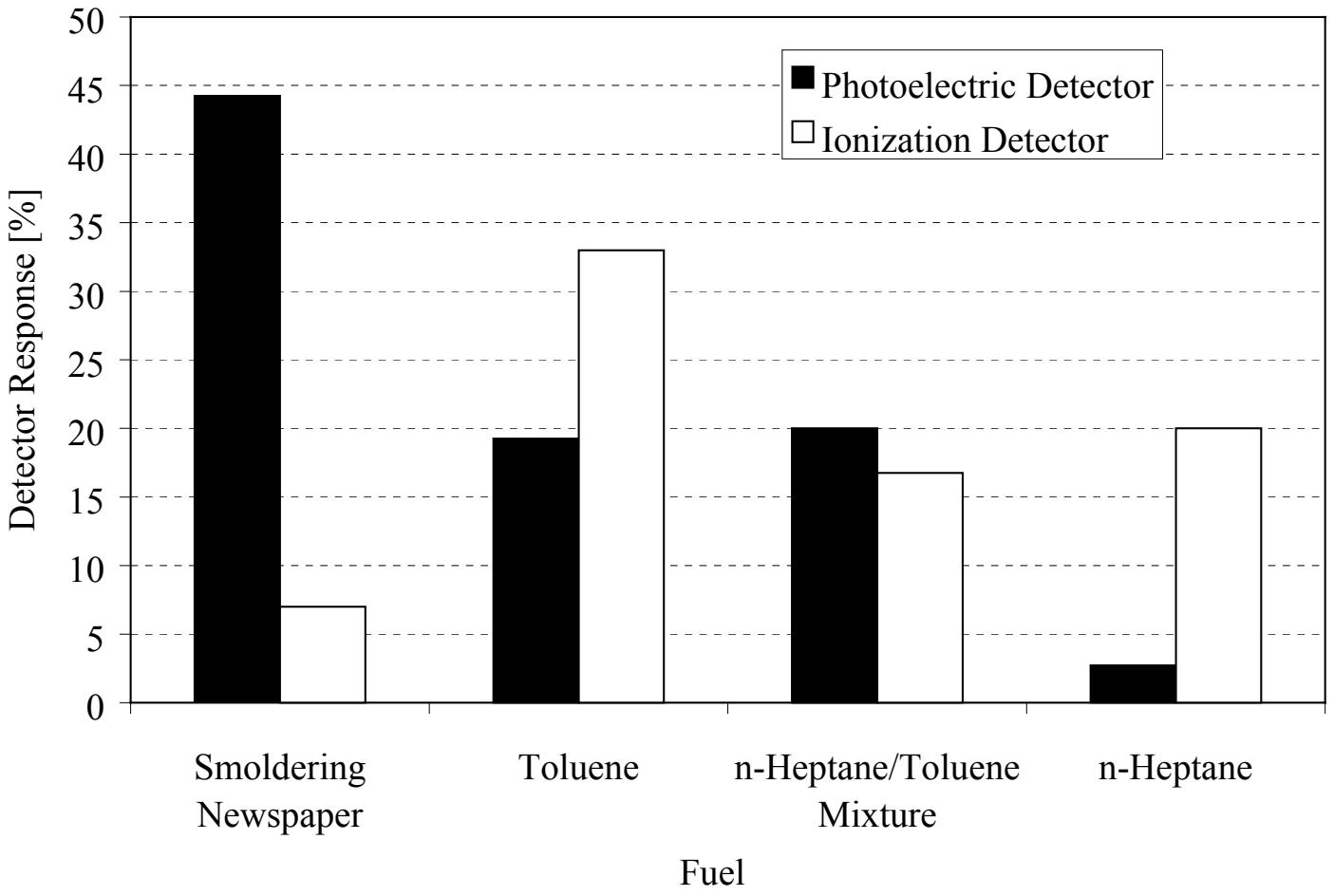

Wolin et al.
Figure 6

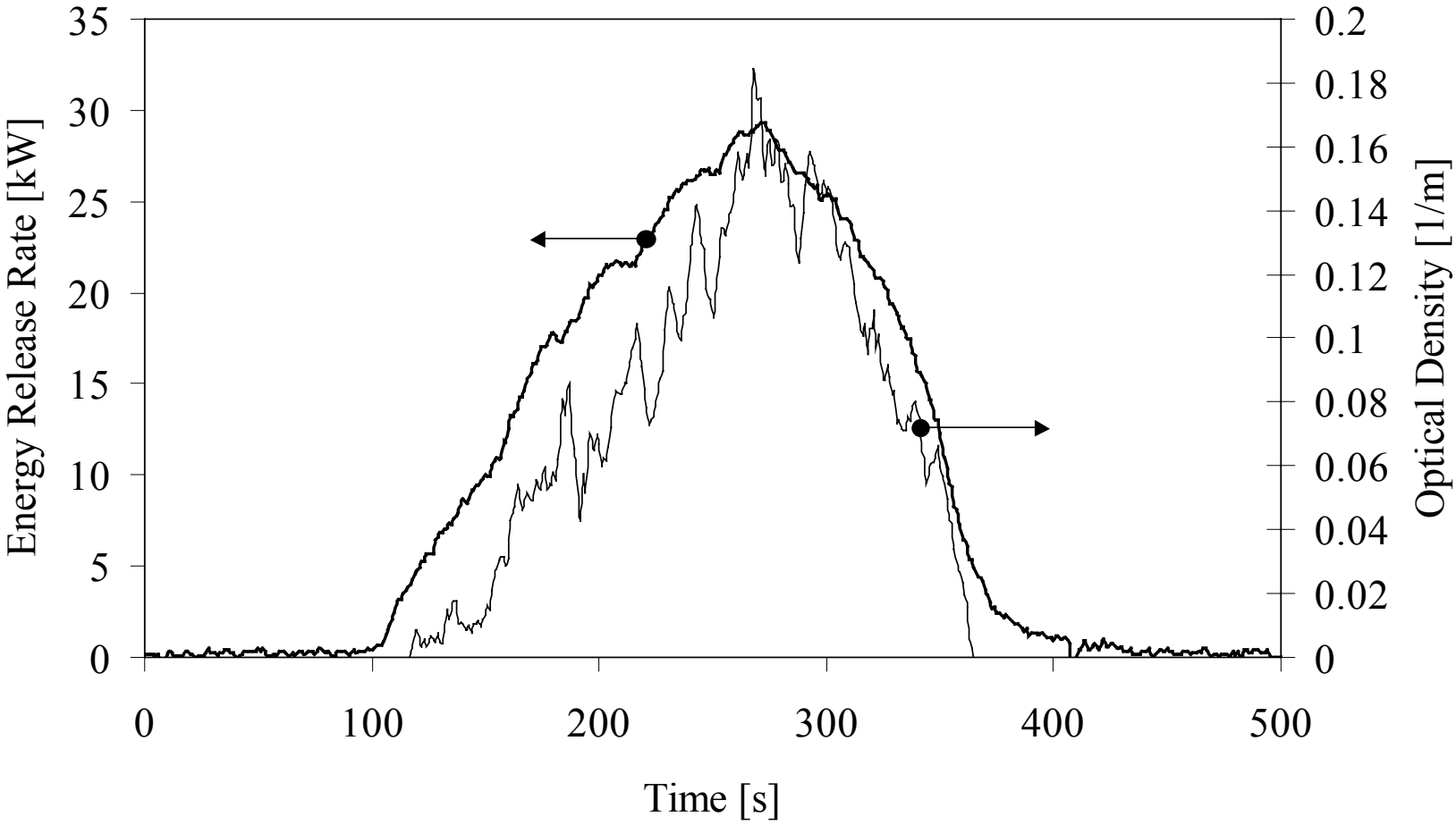

Wolin et al.
Figure 7

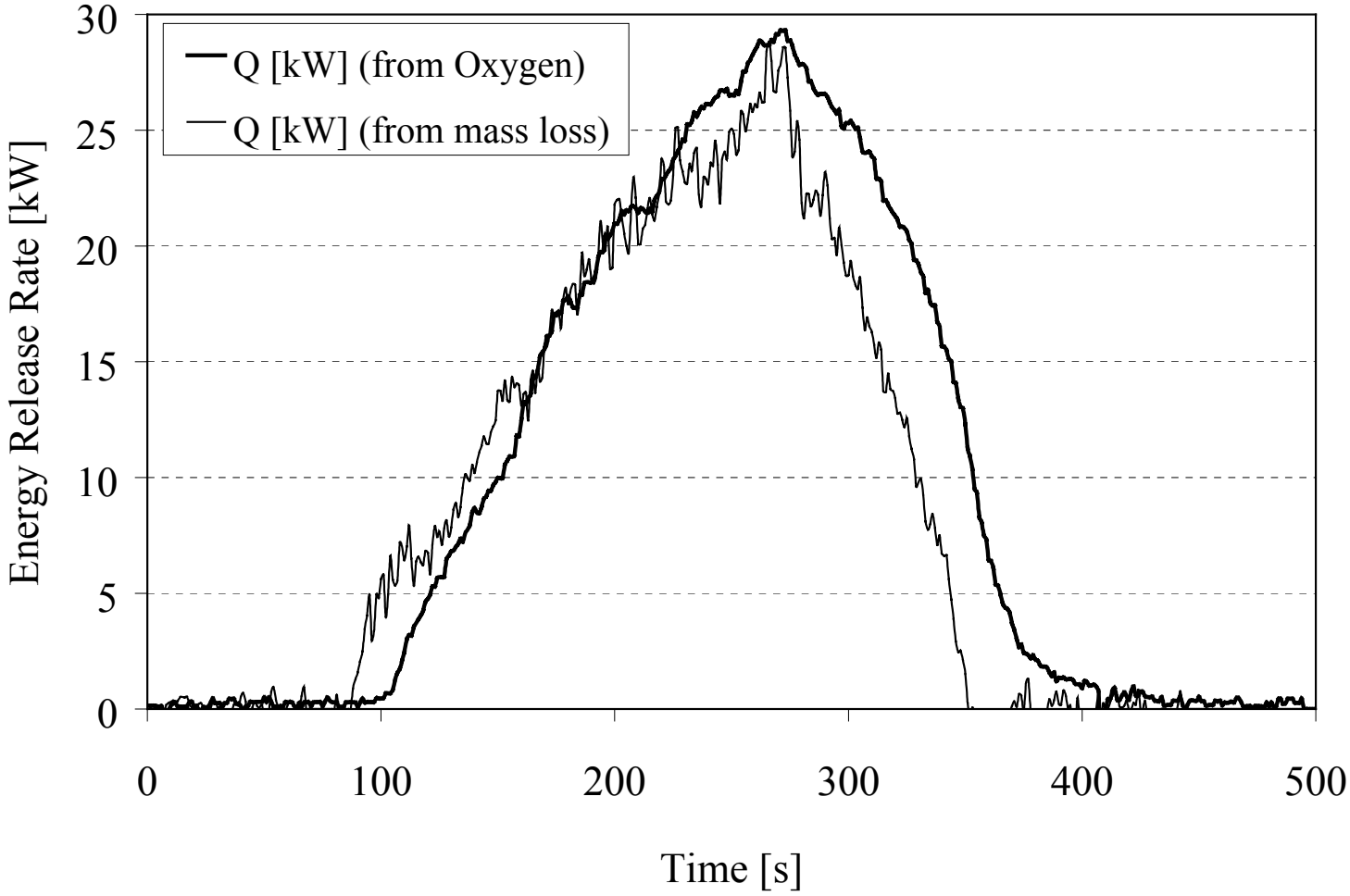

Wolin et al.
Figure 8

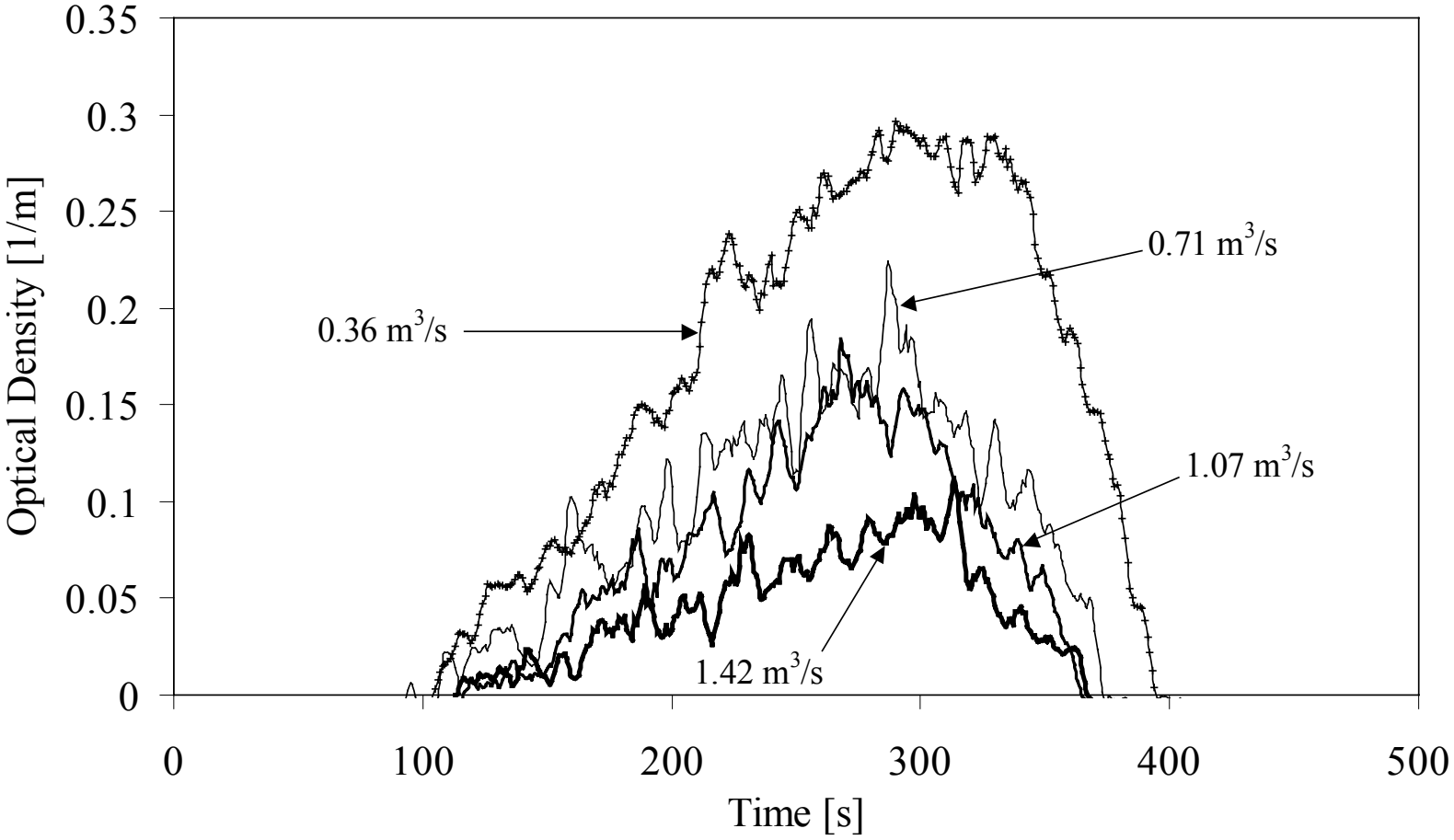

Wolin et al.
Figure 9

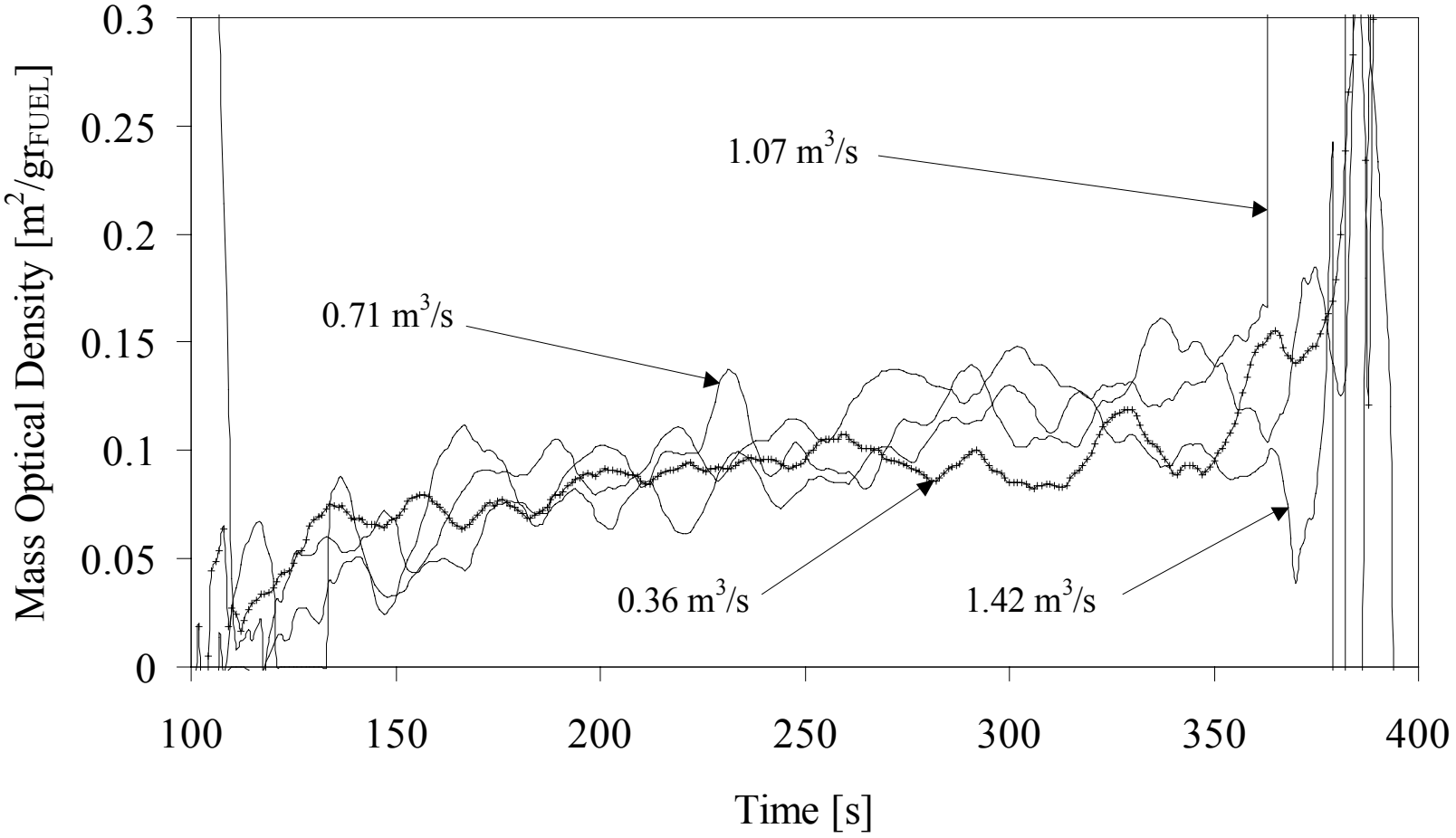

Wolin et al.
Figure 10

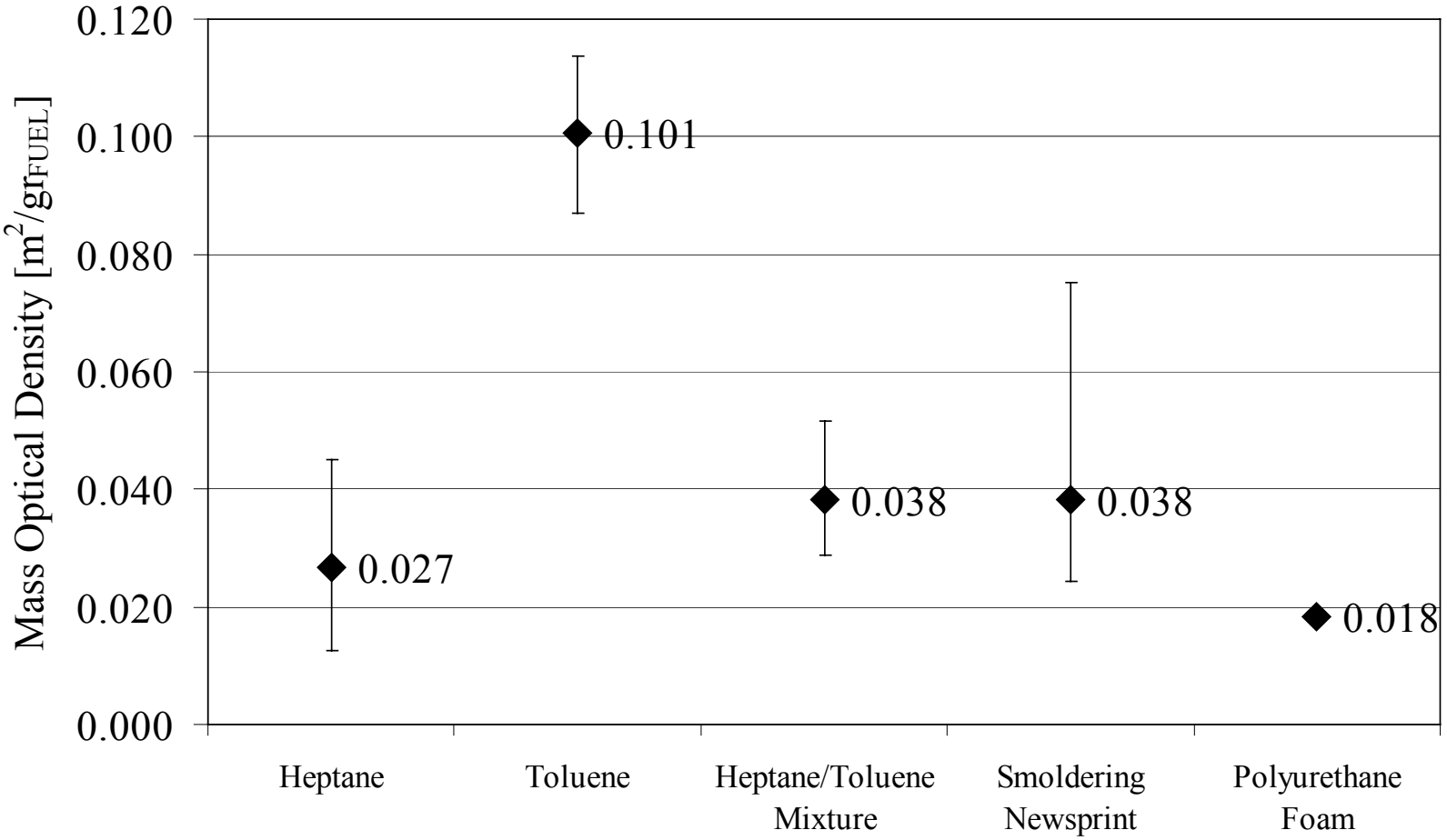

Wolin et al.
Figure 11

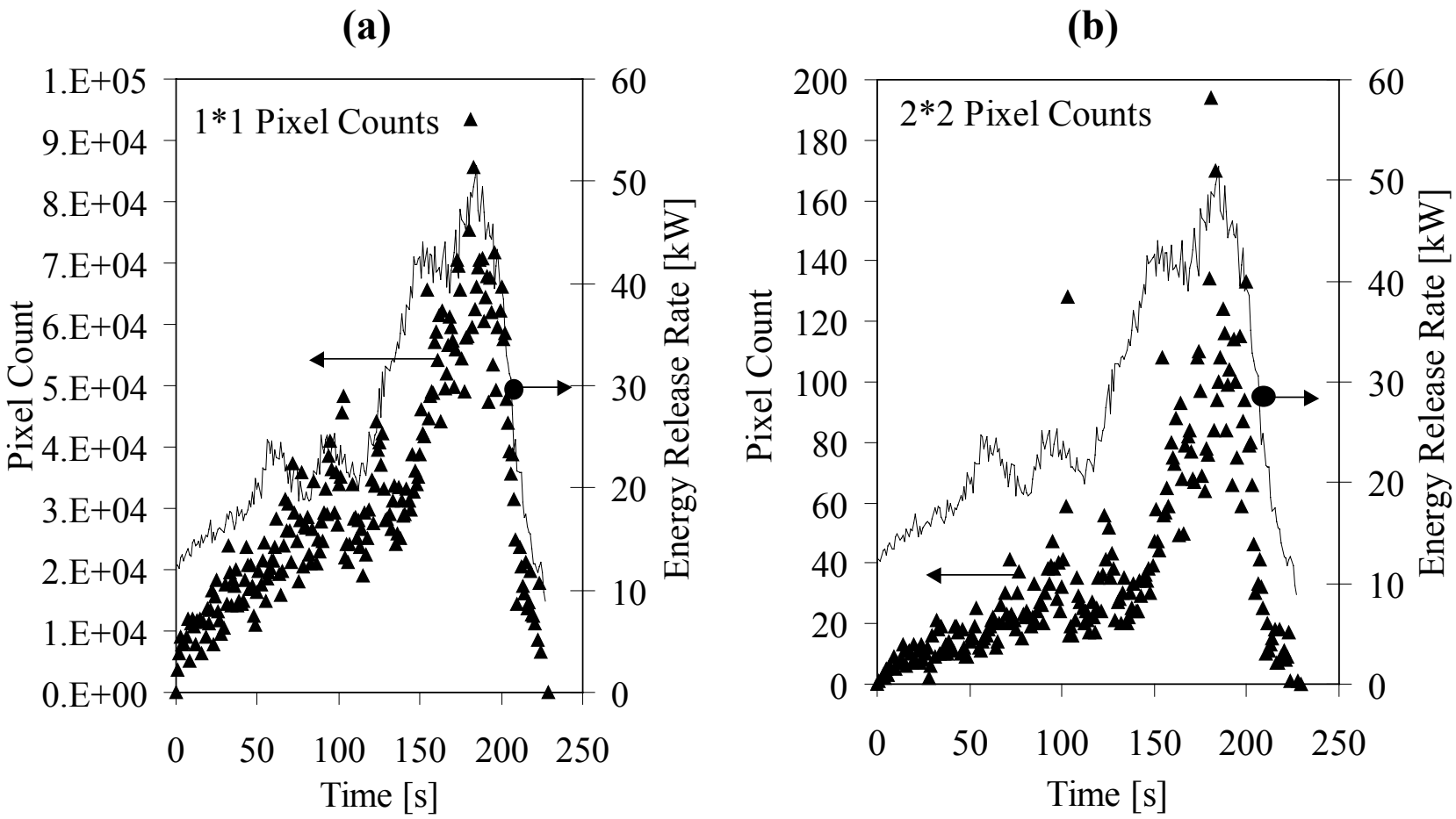

Wolin et al.
Figure 12

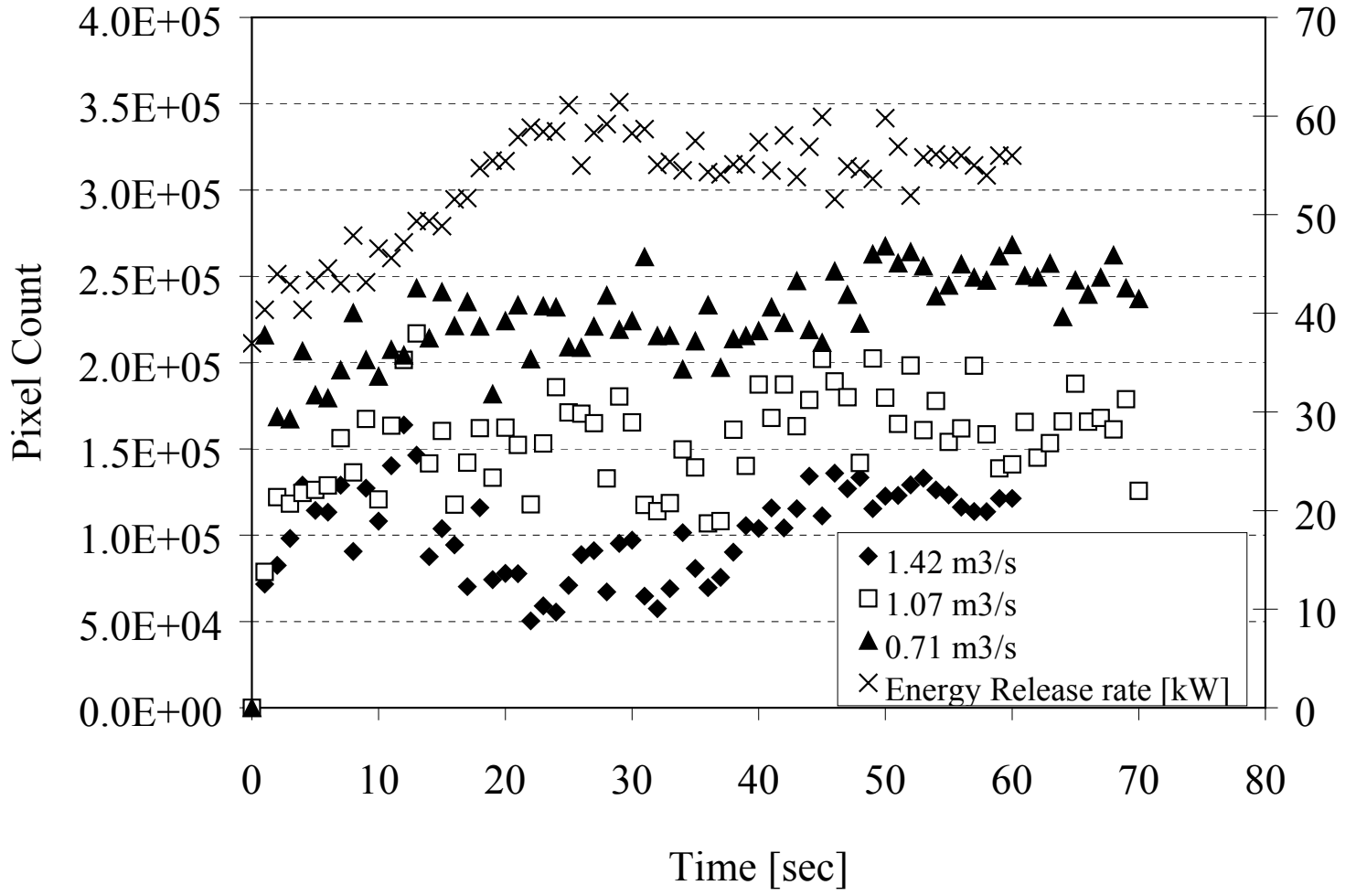

Wolin et al.
Figure 13

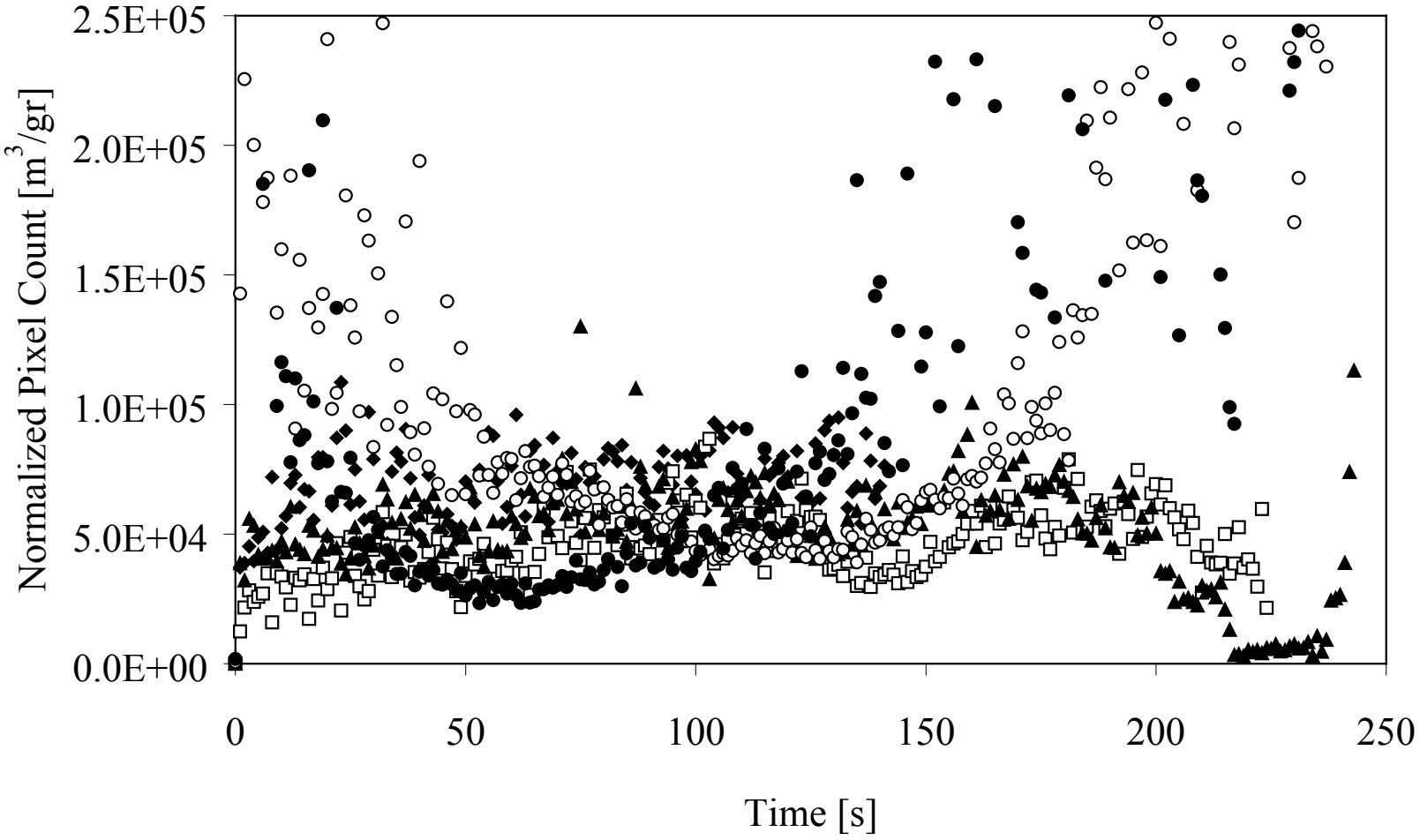

Wolin et al.
Figure 14

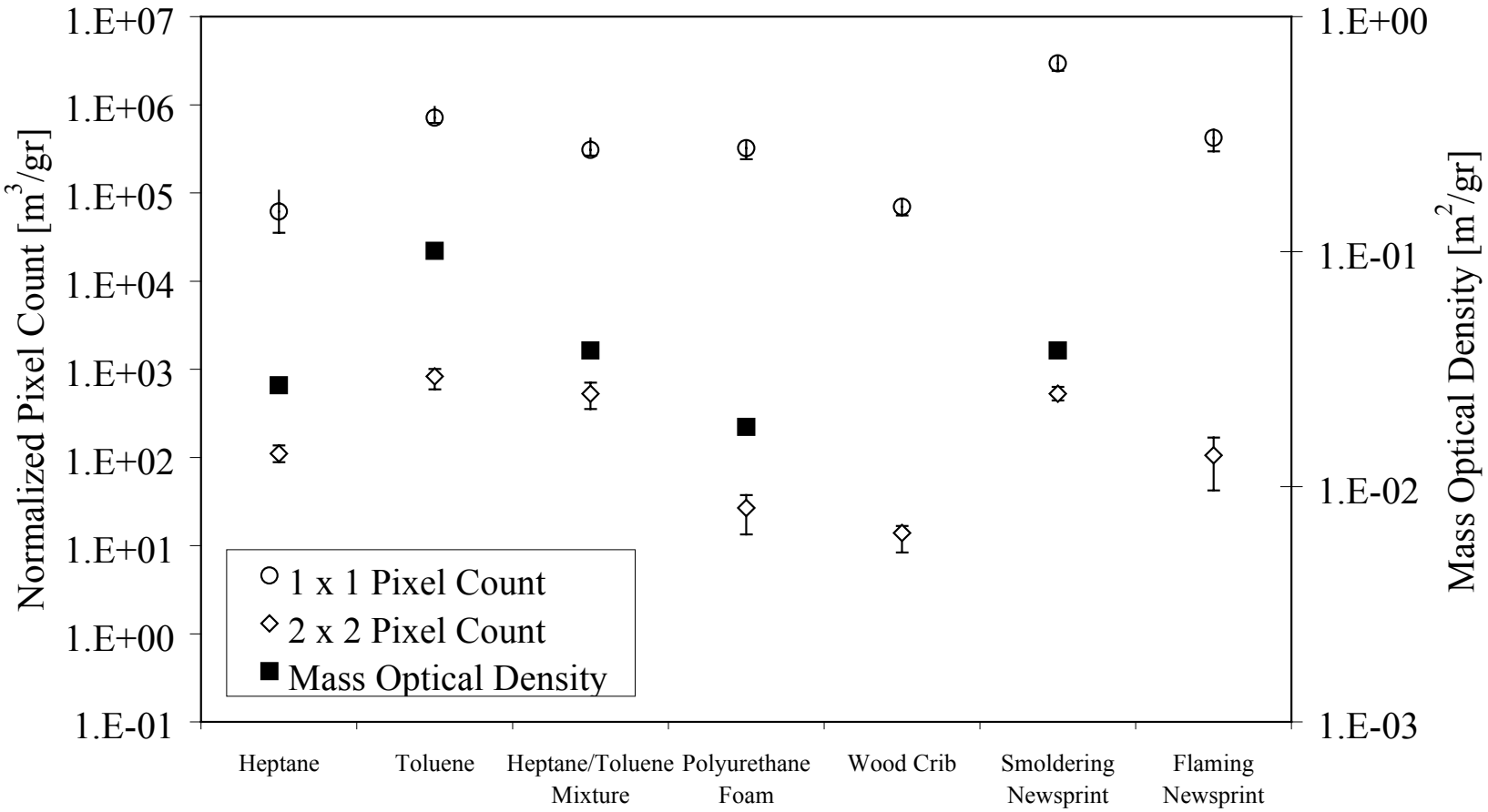

Wolin et al.
Figure 15

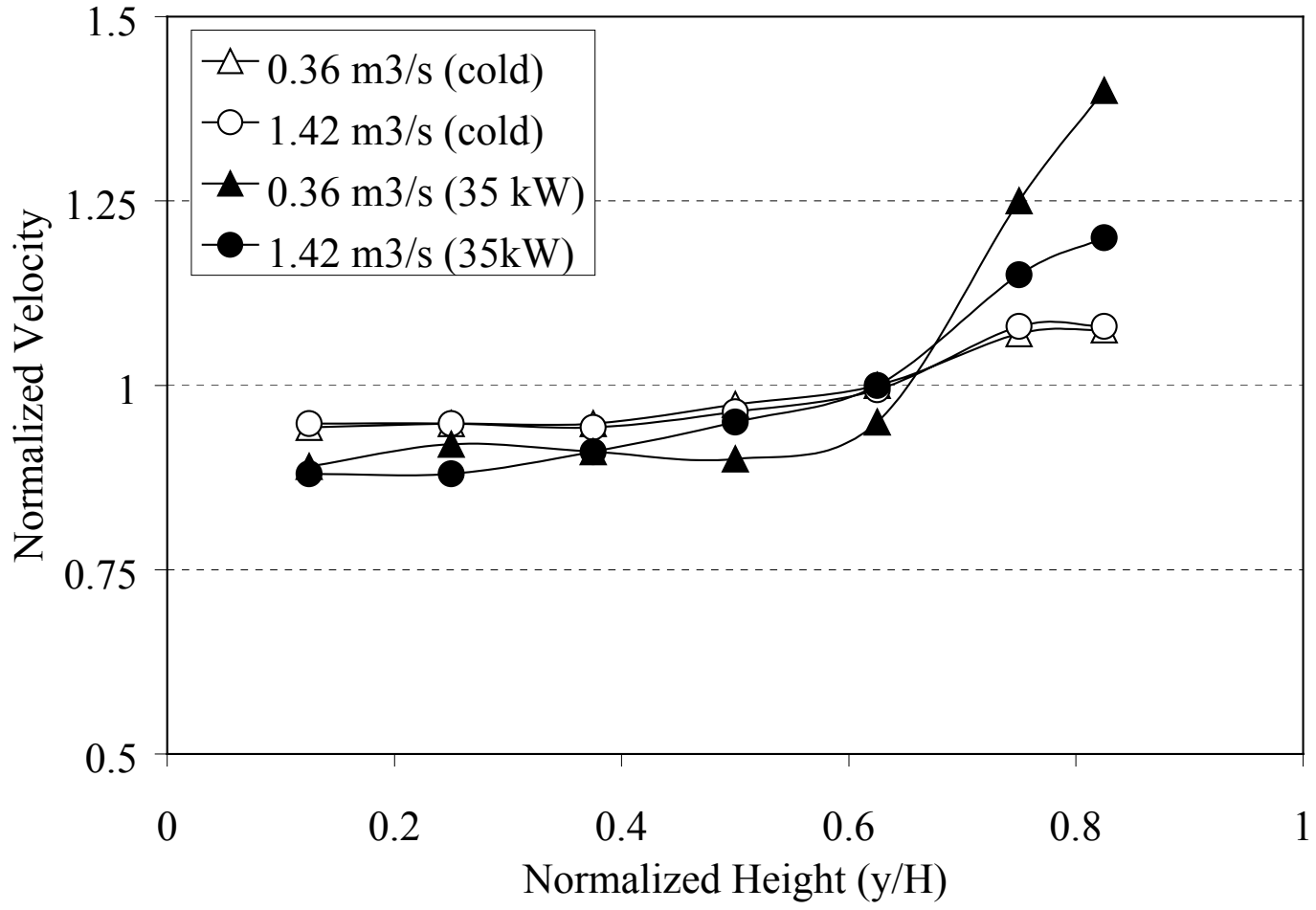

Wolin et al.
Figure 16

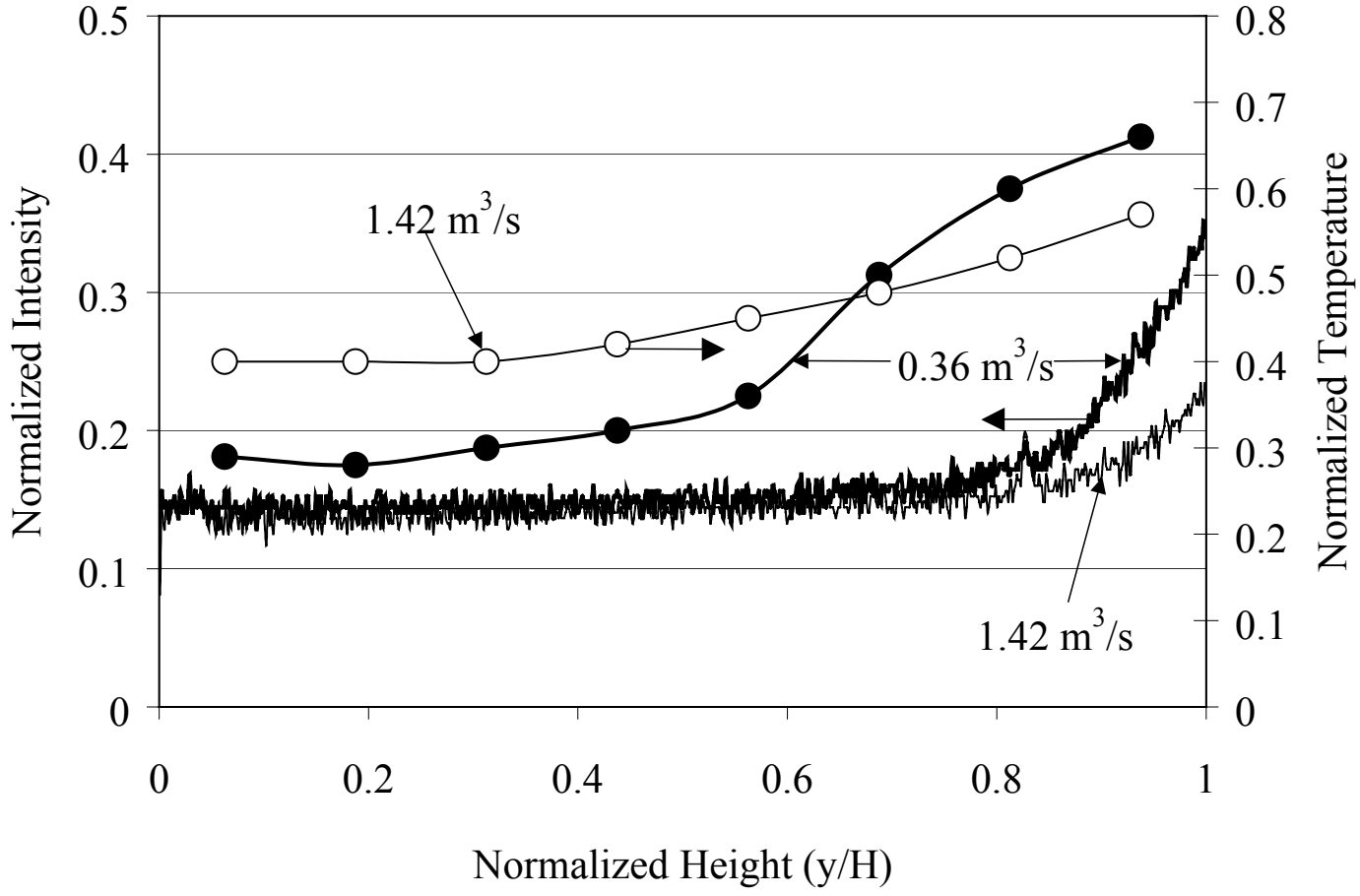

Wolin et al.
Figure 17

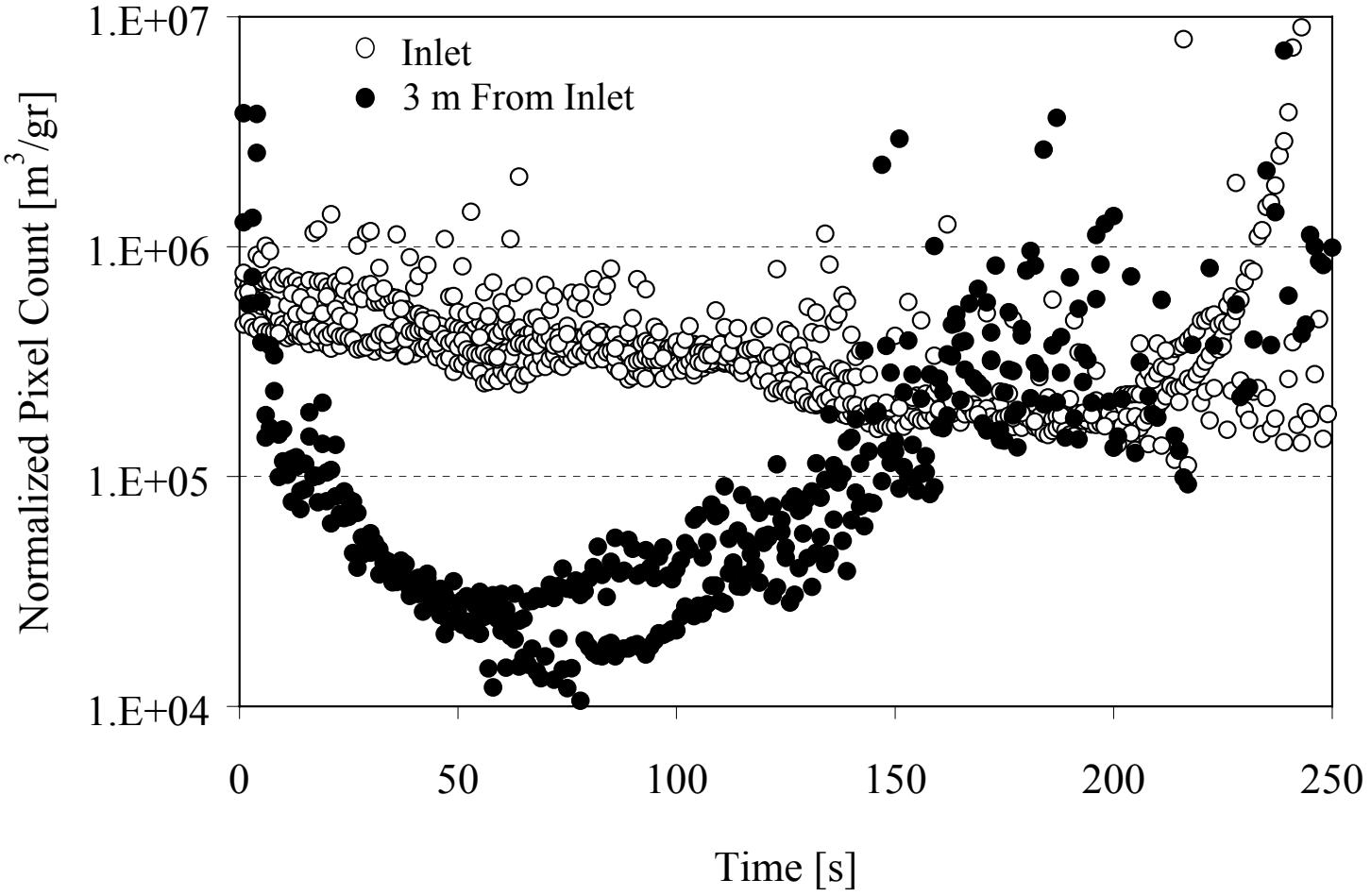

Wolin et al.
Figure 18

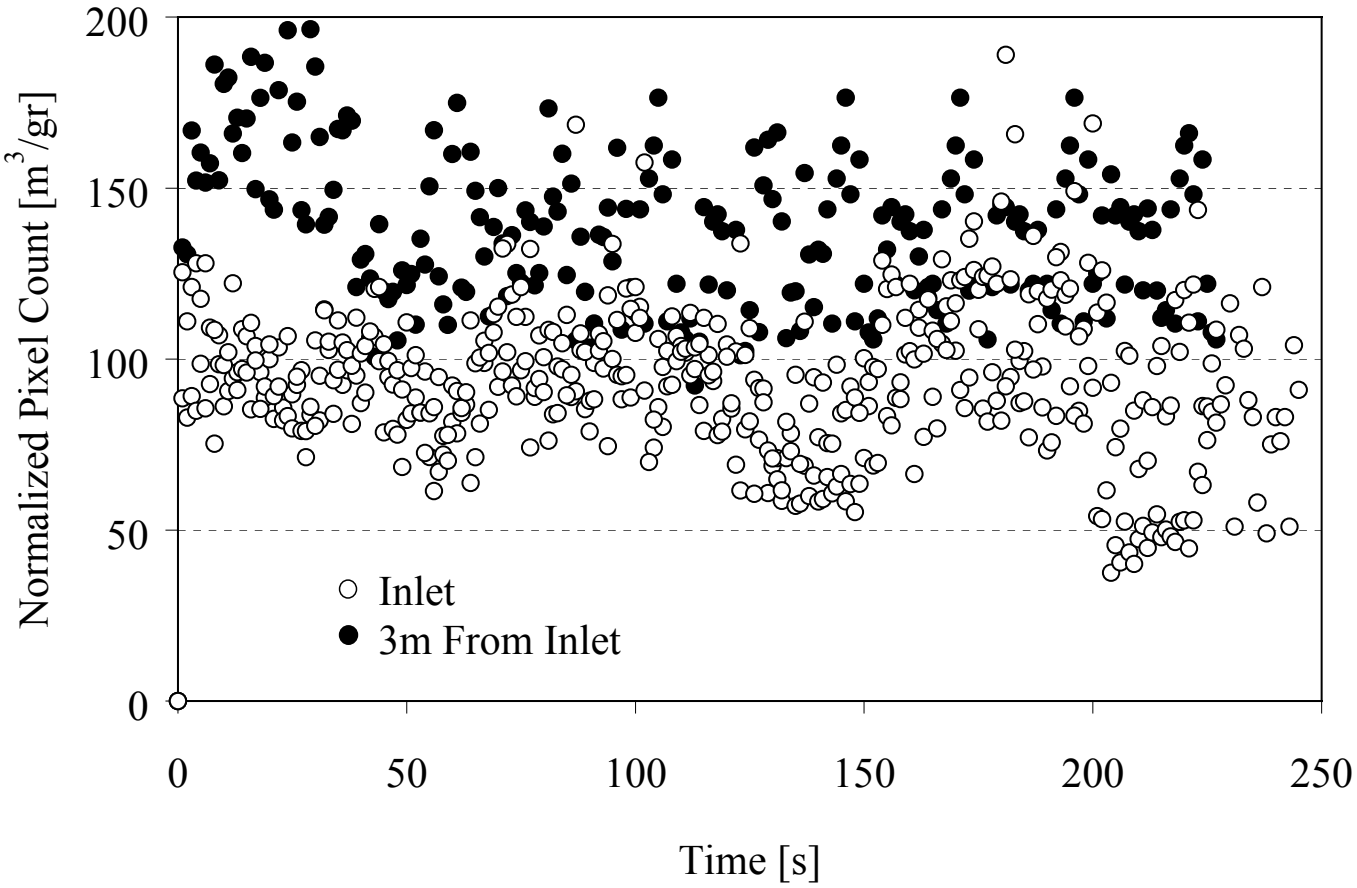

Wolin et al.
Figure 19